ELECTROSTATIC WAVE PHENOMENA IN DUSTY PLASMAS

A DISSERTATION

SUBMITTED TO THE DEPARTMENT OF PHYSICS,

UNIVERSITY OF DURBAN-WESTVILLE

IN PARTIAL FULFILLMENT OF THE REQUIREMENTS

FOR THE DEGREE OF

DOCTOR OF PHILOSOPHY

By

S. Vidhya Lakshmi

May 1995

Preface

The work described in this thesis was carried out by the author in the Department of Physics, University of Durban-Westville, from January 1992 to December 1994, under the supervision of Professor R. Bharuthram.

These studies represent original work by the author and have not been submitted in any form to another university. Where use is made of the work of others, it has been duly acknowledged in the text.

Acknowledgements

With deep sincerity I would like to thank the following people:

My supervisor, Professor R. Bharuthram for his inspiring guidance, interest, encouragement and availability.

Dr P.K. Shukla and Dr M.Y. Yu of Ruhr University, Bochum, Federal Republic of Germany and Dr N.N. Rao of the Physical Research Laboratory, Ahmedabad, India for their helpful and highly informative discussions.

My friend, Thiagan for his kind assitance in resolving problems experienced with plotting graphs and the Latex programme.

My colleagues in the Department of Physics for their concern and interest.

My father for his kind encouragement, interest and prayers and my mother for her love and support when I most needed it. My brothers and sisters for their kind help and prayers.

To all of the above and many other well wishers my sincerest thanks and appreciation.

Dedicated to my loving parents

Abstract

This thesis is concerned with the some aspects of electrostatic wave phenomena dusty plasmas. In particular Debye shielding, nonlinear potential structures such as diploar vortices and solitons are investigated.

The phenomenon of Debye shielding is investigated in a dusty plasma where electrons and ions have Boltzmann density distributions and the massive, negatively charged dust grains are taken to be stationary. Small and large amplitude electrostatic potentials are considered. The existence of nonlinear dipolar-vortex and modified convective cell structures are examined in an inhomogeneous magnetized dusty plasma. A study is carried out on arbitrary amplitude rarefactive and compressive solitons in dusty plasmas. Using the reductive perturbation technique, the kinetic Korteweg-de Vries equation and the corresponding equation for fluid theory is derived. The investigation is done on weak (or small amplitude) solitons. Comparisons between the associated soliton profiles are presented.

List of commonly used symbols

α_f	coefficient of the nonlinear term in fluid KdV
α_j	$= T_{eff}/Z_d T_j$ = ratio of the effective temperature to temperature of the species j (for $j = e, c, h$ for the electrons, cool ions and hot ions respectively)
α_k	coefficient of the nonlinear term in kinetic KdV
$\vec{B}_o$	external magnetic field in the $\hat{\mathbf{z}}$ direction
C_s	$= (T_e/m_i)$ ion acoustic speed
C_{sd}	$= (T_e/m_d)$ dust acoustic speed
Δ	measure of the wave dispersion
e	magnitude of the electron charge
ϵ	expansion parameter
ϵ_o	permittivity of free space
η	coordinate defining stationary frame
$f_d, f_d(u, \xi, \tau)$	kinetic distribution functions
γ_f	coefficient of the linear term in fluid KdV
γ_k	coefficient of the linear term in kinetic KdV
KdV	Korteweg-de Vries
λ	phase velocity

λ_D	electron Debye length
λ'_D	effective Debye length
M	Mach number
m_j	mass of the species j (for $j = i, d$ for the ions
	and dust particles respectively)
μ_j	magnetic moment of the j^{th} species for $j = i, d$
n'_d	normalised dust number density
n_j	density of the species j (for $j = e, i, d$ for the electrons
	ions and dust particles respectively)
n_{jo}	equilibrium density of the species j
N_{jo}	normalised equilibrium density of the species $j(j = e, c, h, d)$
n_o	$= n_{eo} + Z_d n_{do} = n_{io}$, total plasma density
N_d	total charge within Debye sphere
Ω_j	gyrofrequency of the j^{th} species $j = i, d$
ω_{pd}	dust plasma frequency
ϕ	electrostatic potential
ϕ_m	soliton amplitude maximum
ψ	$= (\lambda_d \phi / e)$ dimensionless variable [chapter two]
$\psi(\phi)$	Sagdeev potential
r, θ	polar coordinates
R	vortex radius
R^{-1}	magnetic curvature
ρ	$= (r/\lambda_d)$dimensionless variable
σ	$= T_e/T_i =$ ratio of the electron temperature
	to ion temperature

σ_1	$= T_d/T_e$ = ratio of the temperature of the dust to electron temperature
T_c	temperature of the cool ions
T_h	temperature of the hot ions
T_j	temperature of the species $j(j = e, i, d)$
u	velocity of the dust fluid [chapter five]
$\vec{v}_j$	velocity of the species $j(j = i, d$for the ions and dust fluids)
$\vec{V}_E$	$E \times B$ drift
$\vec{V}_{Dj}$	curvature drift
$\vec{V}_{pj}$	polarization drift
ξ	spatial coordinate
Z_d	magnitude of the dust particles charge

Contents

List of Figures

Chapter 1

INTRODUCTION

An ordinary plasma is defined as a quasi-neutral collection of electrons, ions and neutral particles in which the long range electromagnetic forces dominate over the short range billiard ball collisions. In this sense a plasma displays collective behaviour. Quasi-neutrality is associated with the phenomenon of Debye shielding, which is characterized by the Debye length: the typical distance over which any electric potential perturbation (external or internal) is shielded from the rest of the plasma. As a result of the much greater mobility of the electrons the Debye length is usually expressed in terms of the electron parameters, it is given by

$$\lambda_D = \left(\frac{\epsilon_o k T_e}{n_e e^2} \right)^{\frac{1}{2}} , \tag{1.1}$$

where $T_e(n_e)$ is the electron temperature (density), e is the magnitude of the electron charge, ϵ_o the permittivity of free space and k is Boltzmann's constant.

On the other hand, a "dusty plasma" can be generally defined as a plasma with a dispersed phase of solid objects like grains or dust particles. By dust particles we mean particles larger than ionic in size but small enough that electromagnetic

forces on the dust have significant effect on their motion. At one (lower) extreme in which the dust becomes molecular ion in size the plasma would be a multicomponent plasma and not a dusty one. Whereas in the other extreme of larger particles, the gravitational forces dominate over the electromagnetic forces.

Dust is quite common throughout the universe. Some well known systems where the presence of dust has been observed are inter-stellar clouds (from star reddening and infrared emission), circum-stellar clouds and the solar system. Larger objects such as meteorites, planetesimals and planets persumably evolved through coagulation of dust. Recent measurements show that the solar system is full of "grains" of various nature, size and origin: micrometeoriods, space debris, man-made pollution etc. Dust is also seen in planetary magnetospheres, including the earth, and in cometary tails. One of the sources of dust in the earth's magnetosphere is man-made pollution in the form of rocket exhausts. These are mainly in the form of aluminium oxide (Al_2O_3). Sources of dust in planetary magnetospheres are interplanetary dust blown off from comets and asteriods. Missions to Jupiter and Saturn in the last decade have proved that their rings are made of a distribution of micron to submicron size dust particles. Recent interest in dusty plasmas have been accelerated by the observation of dust in the environment of comet halley by the Vega and Giotto space probes; in the vicinity of comet Giacobini-Zinner by the ICE satellite; and in the vicinities of Jupiter, Saturn and Uranus by the Voyager spacecraft.

The effect of dust on the structure and the properties of plasmas was recognised in laboratory experiments long before "space dust". Some sources of such dust are: high Z impurities from the walls in Tokamaks; plasma etching techniques and impurities in MHD generators. The sizes of the particles are found to range from tens of Angstroms to several microns, in some cases up to $0.1cm$ depending on the plasma conditions.

A characteristic of a dust grain in a dusty plasma is that its charge is not fixed, being dependent on environmental factors such as the temperature and density of the surrounding plasma, or processes such as photoemission and secondary emission. For charging effects purely due to the surrounding plasma, the electron and ion fluxes to the dust grain's surface are unequal because of the much larger thermal velocity of the more mobile electrons. Hence, the dust grains become negatively charged to equalize the electron and ion thermal fluxes and thereby establish steady state (Figure 1.1). Consequently, in many theoretical studies the dust grains are taken to be negatively charged. For equal electron and ion temperatures (T), the grain potential is given by $e\phi/kT = -2.51$ for a hydrogen plasma and -3.31 for a singly charged oxygen plasma. For $kT = 1eV$, and grain radius $a = 10\mu m$, calculations yield for the charge on the dust grain $Q_d = -1.7 \times 10^4 e$.

On the other hand, if the the primary electrons are sufficiently energetic, they can produce secondary emission which causes the surface potential to become positive. Also, the absorption of solar UV radiation releases photoelectrons, thereby constituting a positive charging current. There are other sources of charging currents, e.g. thermal emission, sputtering and proton-induced secondaries. Figure 1.2 (Goertz 1989) shows the net current as a function of the dust grain's surface potential due to primary electron and ion currents and secondaries. The constant δ_m is a measure of the material properties of the dust grains and is found to be in the range $0.5 \leq \delta_m \leq 30$. From Figure 1.2, it is seen that there are three values of ϕ_d for a steady state ($J_{tot} = 0$) solution. The two extreme values correspond to stable equilibria (with positive and negative charges, respectively), whereas the intermediate equilibrium is unstable. The variation of the dust grain surface potential as a function of plasma temperature ($T_e = T_i = T$) for different values of δ_m is shown in Figure 1.3. The grain is negative

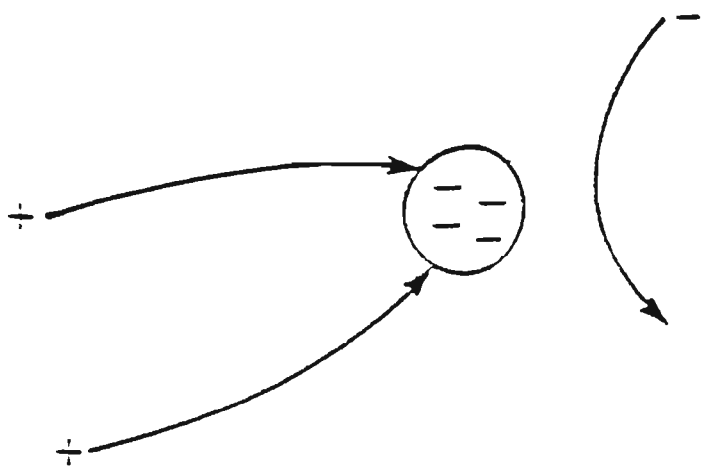

Figure 1.1: A dust grain in a plasma becomes negatively charged.

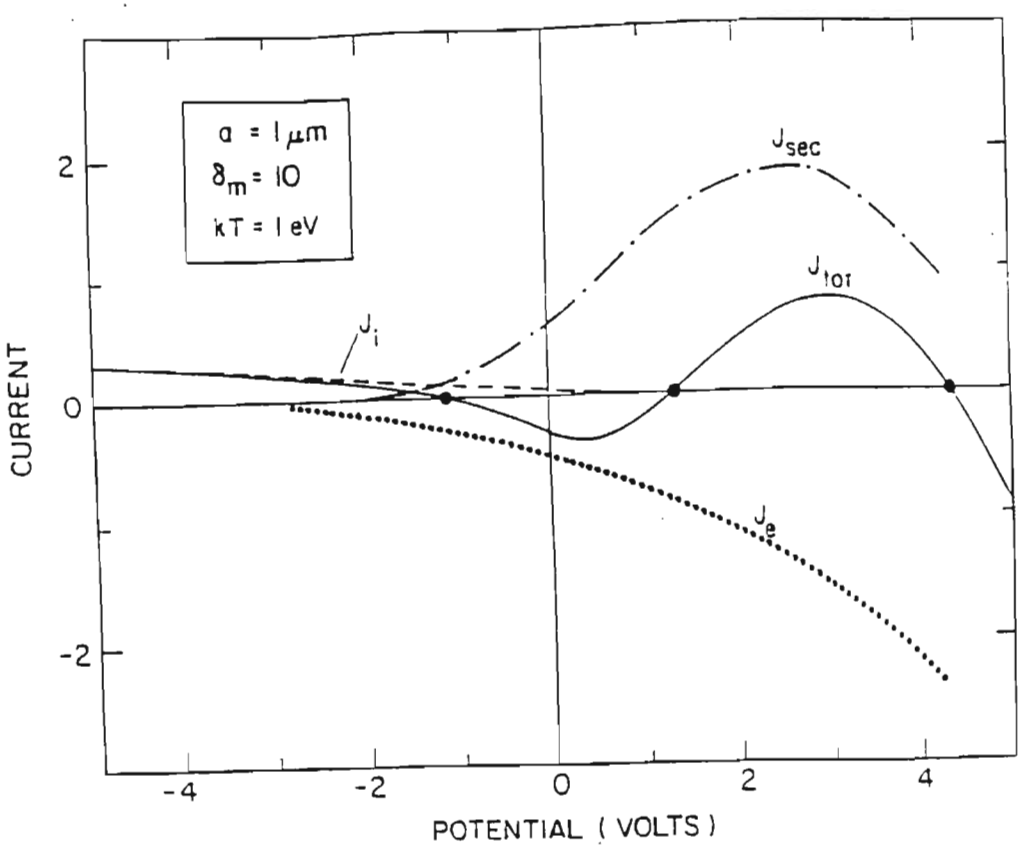

Figure 1.2: The charging current density due to plasma electrons (dotted curve), plasma ions (dashed curve), and secondaries (dashed-dotted curve) as a function of the grain's surface potential ϕ_s. The solid curve is the net charging current density including secondaries for $\delta_m = 10$ and $kT = 1eV$ and the equilibrium surface potential is given by the zeros of the net charging current (from Goertz 1989).

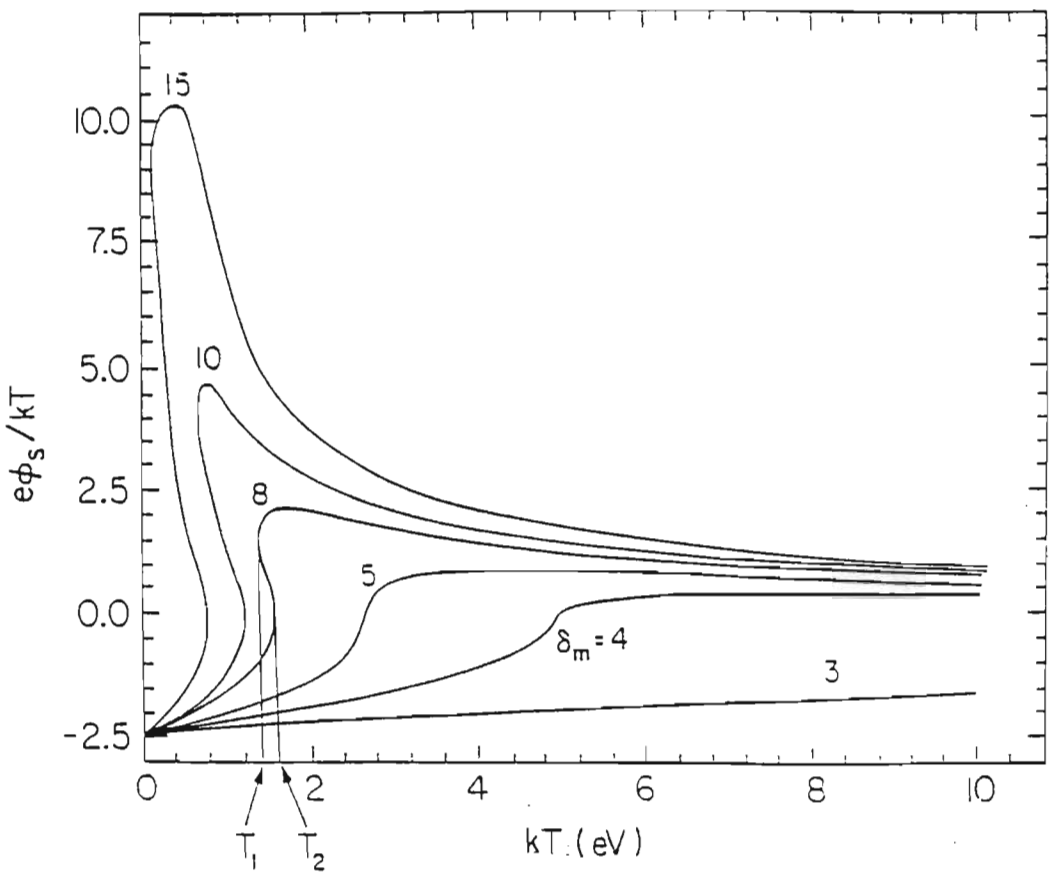

Figure 1.3: The equilibrium surface potential ϕ_s as a function of plasma temperature T for different values of the secondary yield parameter δ_m (from Goertz 1989).

for a cold plasma (T small), because the flux of secondaries is small. But in a hot plasma the flux of secondaries exceeds the flux of primaries thereby resulting in a positive grain potential. This type of behaviour suggests that in a plasma with a fluctuating temperature, some of the dust grains will be positively charged, while others have negative charge.

The charge on the dust can be modified through their motion in a plasma. As the electron thermal velocity is much larger than the dust grain drift velocity, the electron flux is not affected generally by this motion. Since the dust particles are charged, they will be affected by the electric and the magnetic fields often in subtle and surprising ways. In addition, they may change the properties of the plasma itself and change the dispersion relation of various, usually low frequency plasma waves. Depending on the concentration, one can look at either the dust grains in a plasma from a particle dynamics point of view or at the collective effects of the charged dust on the plasma.

In this thesis we study electrostatic wave phenomena in dusty plasmas, in particular Debye shielding and nonlinear potential structures such as dipolar vortices and solitons.
This thesis is organized as follows:-

In Chapter Two the phenomenon of Debye shielding is investigated in a dusty plasma having Boltzmann density distributions for electrons and ions, while the massive, negatively charged dust grains are taken to be stationary. Both small and large amplitude electrostatic potentials are considered.

Chapter Three examines the existence of nonlinear dipolar-vortex and modified convective cell structures in an inhomogeneous magnetized dusty plasma.

Chapter Four presents a study of arbitrary amplitude compressive and rarefactive solitons in dusty plasmas for the plasma model used in chapter two.

Chapter Five, which is concerned with weak (or small amplitude) solitons, contains the derivation of the kinetic KdV equation for dusty plasmas. The corresponding equation for fluid theory is also derived. Comparisons between the associated soliton profiles are presented.

Chapter Six is the concluding chapter in which the summary of our investigations are presented.

Chapter 2

DEBYE SHIELDING IN A DUSTY PLASMA

2.1 Introduction

Firstly, this chapter describes the phenomenon of Debye shielding in a plasma. Then the effect of Debye shielding is examined in a dusty plasma in which the thermal electrons and ions have been taken as point particles having Boltzmann density distributions, while the massive, negatively charged dust grains are stationary. An analytical expression is derived for the one- dimensional effective Debye length for the case of small amplitude potentials. Then an approximate analytical solution of the Poisson equation, using spherical coordinates, is compared with a numerical solution of the complete equation using a backward differencing scheme.

It is well known that in an electron-ion plasma, electrons are attracted to the vicinity of an ion and shield its electrostatic field from the rest of the plasma. Similarly, an electron at rest repels other electrons and attracts ions. The formation of a shielding

cloud of charge takes place over a typical distance defined as the Debye length λ_D (Chen, 1974), which is given by

$$\lambda_D = \left(\frac{T_e}{4\pi n_o e^2}\right)^{\frac{1}{2}} . \tag{2.1}$$

Here T_e is the electron temperature, n_o the equilibrium density of the electrons(and ions)

In a dusty plasma, for example, a negatively charged dust, tends to attract the positive ions and repel the negative electrons. This positive charge density partially shields out the negative dust charge and reduces the electric field significantly. This "Debye shielding" effect is a unique consequence of the fact that the dust is immersed in a plasma.

Using a scaling technique, the assumption $e\phi \ll kT$ for weak potentials is put in perspective by Mak (1992) who has shown that the linearized solution we are accustomed to remains valid well after the linearization is violated. In this chapter, we extend his work to the case of a dusty plasma.

2.2 Theory

In our model both the positive ions and the electrons are treated as point particles in comparison to the massive dust particles. Hence, allowing for finite electron and ion temperatures, the number density of both the species is taken to be of the Boltzmann type (Rao et. al, 1990; Bharuthram and Shukla, 1992). The dust grains are assumed to be cold. Furthermore, becausé of their large mass they are assumed not to participate in the motion over the time scale involved, thereby forming a neutralizing background.

2.2.1 Weak electrostatic potentials

We begin by deriving an expression for the Debye length in a dusty plasma following the usual 'weak' potential expansion technique (Chen, 1974). As stated above, in our model both the electrons and the ions are treated as point particles with Boltzmann density distributions (Rao et. al, 1990; Bharuthram and Shukla, 1992) given by, respectively,

$$n_e = n_{eo}\, exp(e\phi/T_e)\,, \tag{2.2}$$

and

$$n_i = n_{io}\, exp(-e\phi/T_i)\,, \tag{2.3}$$

where ϕ is the electrostatic potential and T_j is the temperature of species j ($j = e(i)$ for the electrons (ions). Quasineutrality at equilibrium requires that the equilibrium densities n_{jo} satisfy

$$n_{eo} + Z_d n_{do} = n_{io} = n_o\,, \tag{2.4}$$

where n_{do} is the density of the negatively charged dust particles, Z_d the magnitude of their charge, and n_o is the total plasma density.

The system of equations is closed with Poisson's equation

$$\nabla^2\phi = 4\pi e(n_e + Z_d n_d - n_i). \tag{2.5}$$

For $\mid e\phi/T_j \mid \ll 1\,(j = e, i)$, we expand the exponential terms in (2.2) and (2.3). Upon then combining with (2.4) and (2.5) one obtains

$$\nabla^2\phi = 4\pi n_{eo} e \left(1 + \frac{n_o}{n_{eo}}\frac{T_e}{T_i}\right)\frac{e\phi}{T_e}\,. \tag{2.6}$$

We note that in arriving at (2.6) the massive dust grains have been assumed to be stationary charged particles.

Restricting the analysis to one dimension, (2.6) is easily solved in Cartesian coordinates to yield

$$\phi = \phi_o \, exp(-x/\lambda'_D) \, , \tag{2.7}$$

where the effective Debye shielding distance is

$$\lambda'_D = \frac{\lambda_D}{\left[\frac{n_{eo}}{n_o} + \frac{T_e}{T_i}\right]^{\frac{1}{2}}} \, , \tag{2.8}$$

where $\lambda_D = (T_e/4\pi n_o e^2)^{\frac{1}{2}}$ is the usual Debye length in an electron - ion plasma.

In Figure 2.1 is shown the variation of λ'_D/λ_D with the normalized electron density n_{eo}/n_o for different values of the electron to ion temperature ratios T_e/T_i. Here we set $Z_d = 100$, and vary n_{do}/n_o from 0.0005 to 0.0095. It is observed that the effective Debye length in a dusty plasma is smaller than that for an ordinary electron - ion plasma, the relative fraction decreasing with increasing values of the temperature ratio T_e/T_i. For $T_e/T_i \geq 10$, an increase in the electron density has little effect on the effective Debye length. This may be attributed to the electrons being very energetic at such temperatures, thus they are easily repelled by the negatively charged dust grains. For the massive, stationary dust grains the shielding is then essentailly provided by the positive (point particle) ions.

2.2.2 Large amplitude electrostatic potentials

Here, we examine the validity of the assumption $\mid e\phi/T_j \mid \ll 1 \, (j = e, i)$ used in obtaining (2.6) and (2.7) by solving the appropriate Poisson equation numerically. In doing so we use spherical coordinates. For $\phi = \phi(r)$, the approximate equation (2.6) yields

$$\phi(r) = \hat{\phi}_o \frac{exp(-r/\lambda'_D)}{r/\lambda'_D} \, , \tag{2.9}$$

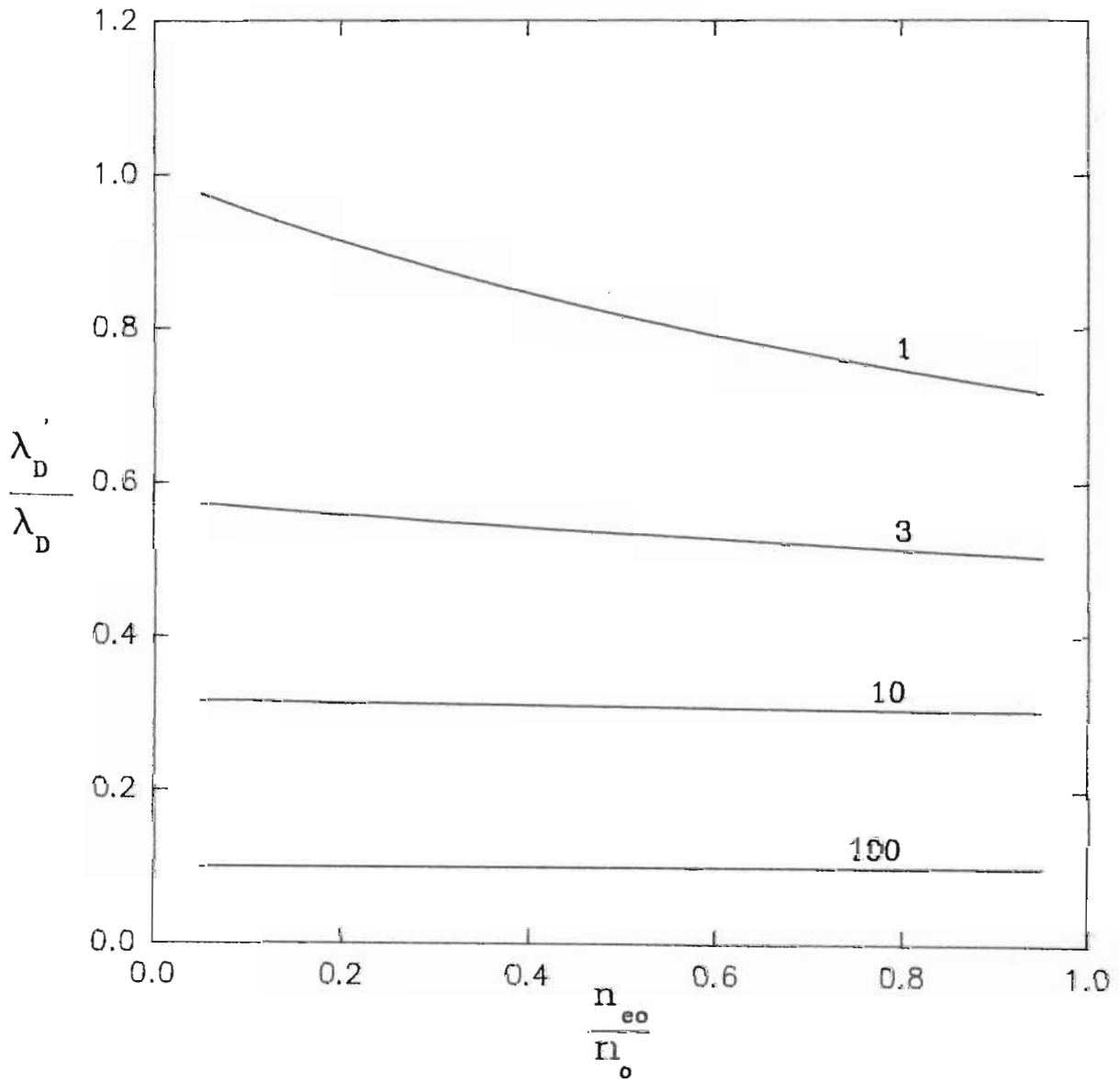

Figure 2.1 : The variation of λ'_D/λ_D with the normalized electron density. The parameter labelling the curves is the electron to ion temperature ratio T_e/T_i.

where $\hat{\phi}_o = e\phi_o$, with $\phi = \phi_o$ at $r = \lambda'_D$.

Let us now consider the complete equation (2.5). In solving it numerically we follow the technique of Mak (1992). In spherical coordinates, with the dimensionless variables $\rho = r/\lambda_D$ and $\psi = \lambda_D\phi/e$, (2.5) can be written as

$$\partial_\rho^2(\rho\psi) = -N_d\rho\left\{\frac{n_{eo}}{n_o}\left[1 - exp(\frac{\psi}{N_d})\right] - \left[1 - exp(-\frac{\psi}{N_d}\frac{T_e}{T_i})\right]\right\}, \qquad (2.10)$$

where $N_d = 4\pi n_o\lambda_D^3$ represents the total charge within a Debye sphere.
Equation(2.10) is solved using a central differencing scheme. With the approximate solution (2.9) as an inital solution at $\rho \rightarrow \infty$, where ϕ is small, a backward differencing scheme (Mak, 1992) is used to numerically calculate the potential at lower ρ values.

Figures 2.2(a) - 2.2(c) present the approximate solution (2.9) as well as the exact numerical solution of (2.10) for $T_e/T_i = 1$, 10 and 100, respectively. Standard parameter values are $Z_d = 100$, $n_o\lambda_D^3 = 30$ and $n_{do}/n_{e0} = 0.005$ (corresponding to $n_{eo}/n_o = 0.5$). It is seen that the difference between the approximate analytical and the numerical solutions become significant for $\rho \leq 0.3$, when the value of the potential begins to rise sharply. As an illustration, for $T_e/T_i = 1$, the approximate value of ϕ is 4% larger than the computed value at $\rho = 0.1$, while for $T_e/T_i = 100$, the approximate value of ϕ is 20% smaller than the computed value at the same value of ρ. However, the shapes of the two curves are similar. The difference in behaviour with varying T_e/T_i, may be attributed to the fact that although the normalized potential satisfies $\mid e\phi/T_e \mid \ll 1$ for all the curves in Figure 2.2, the additional requirement $\mid e\phi/T_i \mid \ll 1$ in obtaining the analytical result (2.9) becomes that more difficult to satisfy as T_e/T_i increases.

The effect of the dust grains on the decaying potential is shown in Figure 2.3, where

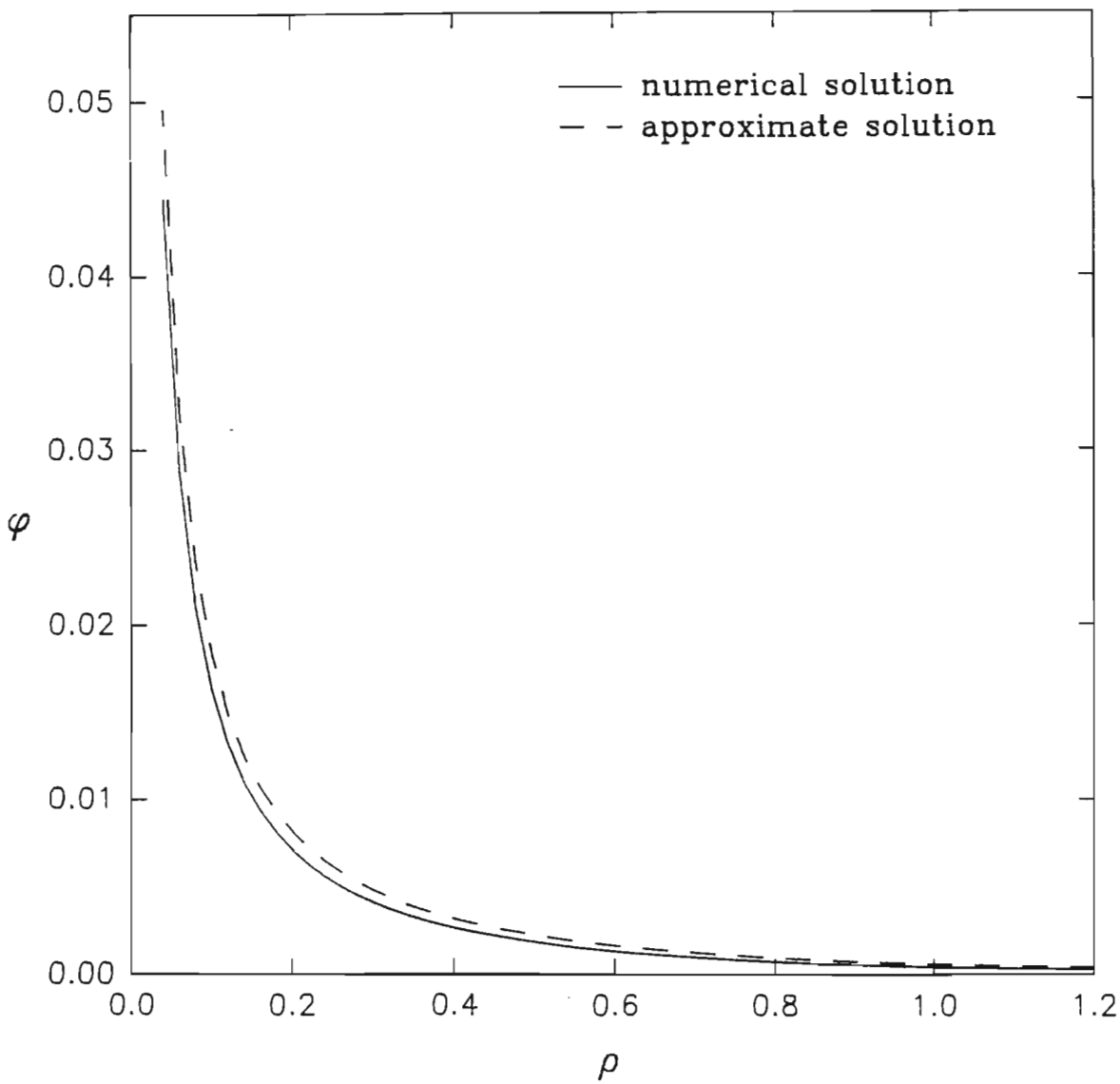

Figure 2.2 a: The approximate solution (2.9) for ϕ and a numerical solution of the complete equation (2.10) for $T_e/T_i = 1$. Here we set $n_{do}/n_o = 0.005$ ($n_{eo}/n_o = 0.5$).

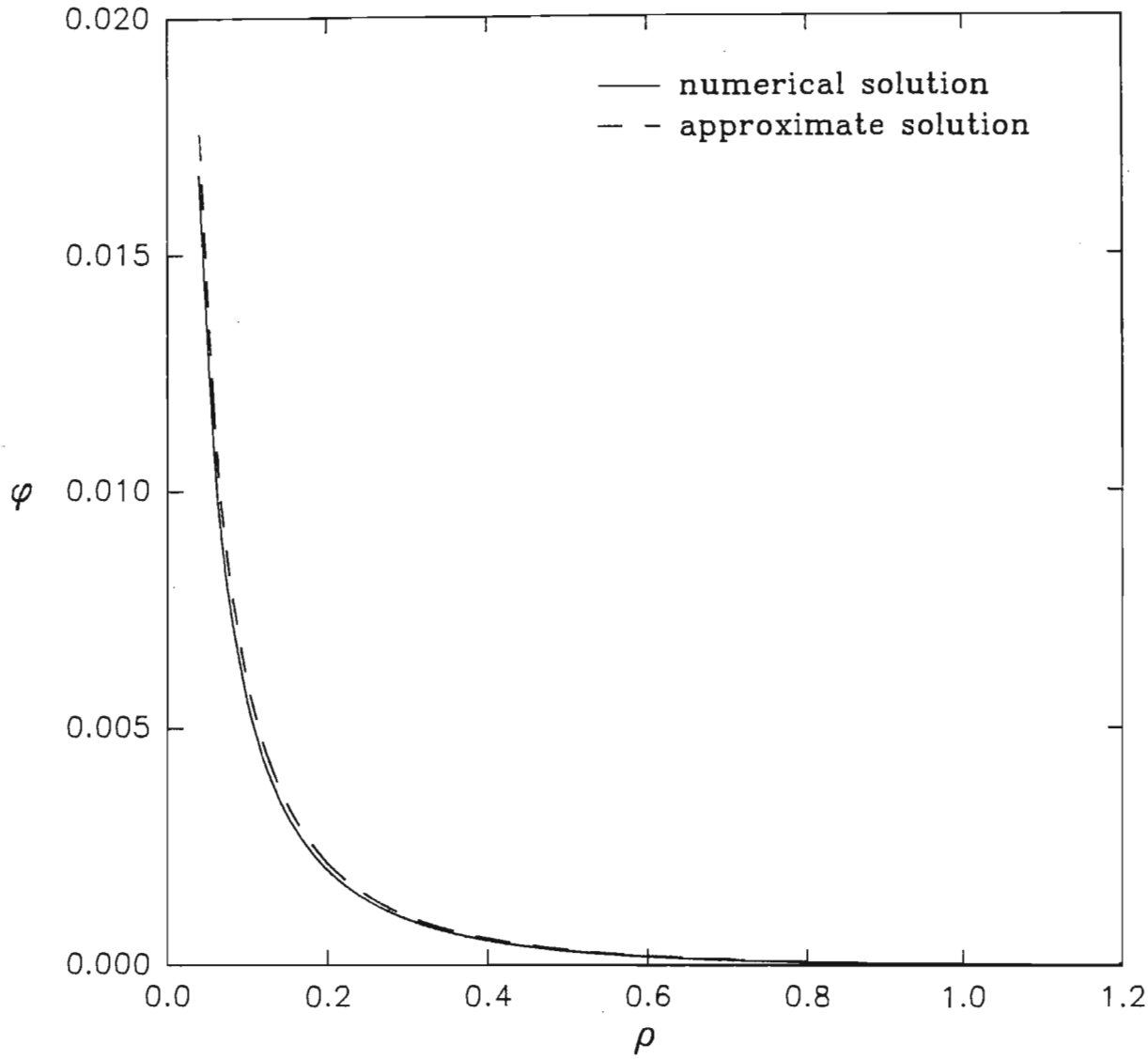

Figure 2.2 b: The approximate solution (2.9) for ϕ and a numerical solution of the complete equation (2.10) for $T_e/T_i = 10$. Here we set $n_{do}/n_o = 0.005$ ($n_{eo}/n_o = 0.5$).

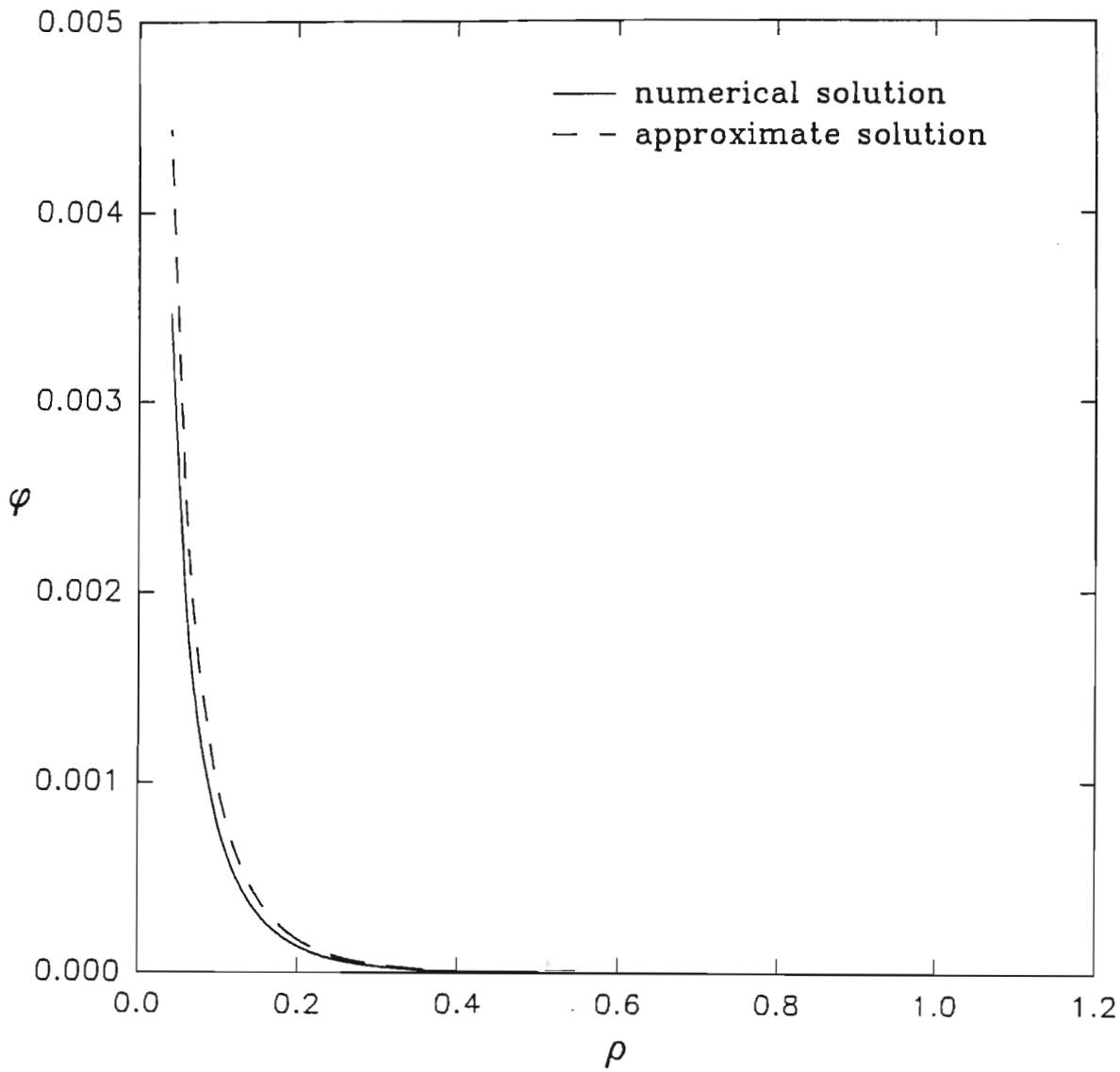

Figure 2.2 c: The approximate solution (2.9) for ϕ and a numerical solution of the complete equation (2.10) for $T_e/T_i = 100$. Here we set $n_{do}/n_o = 0.005$ ($n_{eo}/n_o = 0.5$).

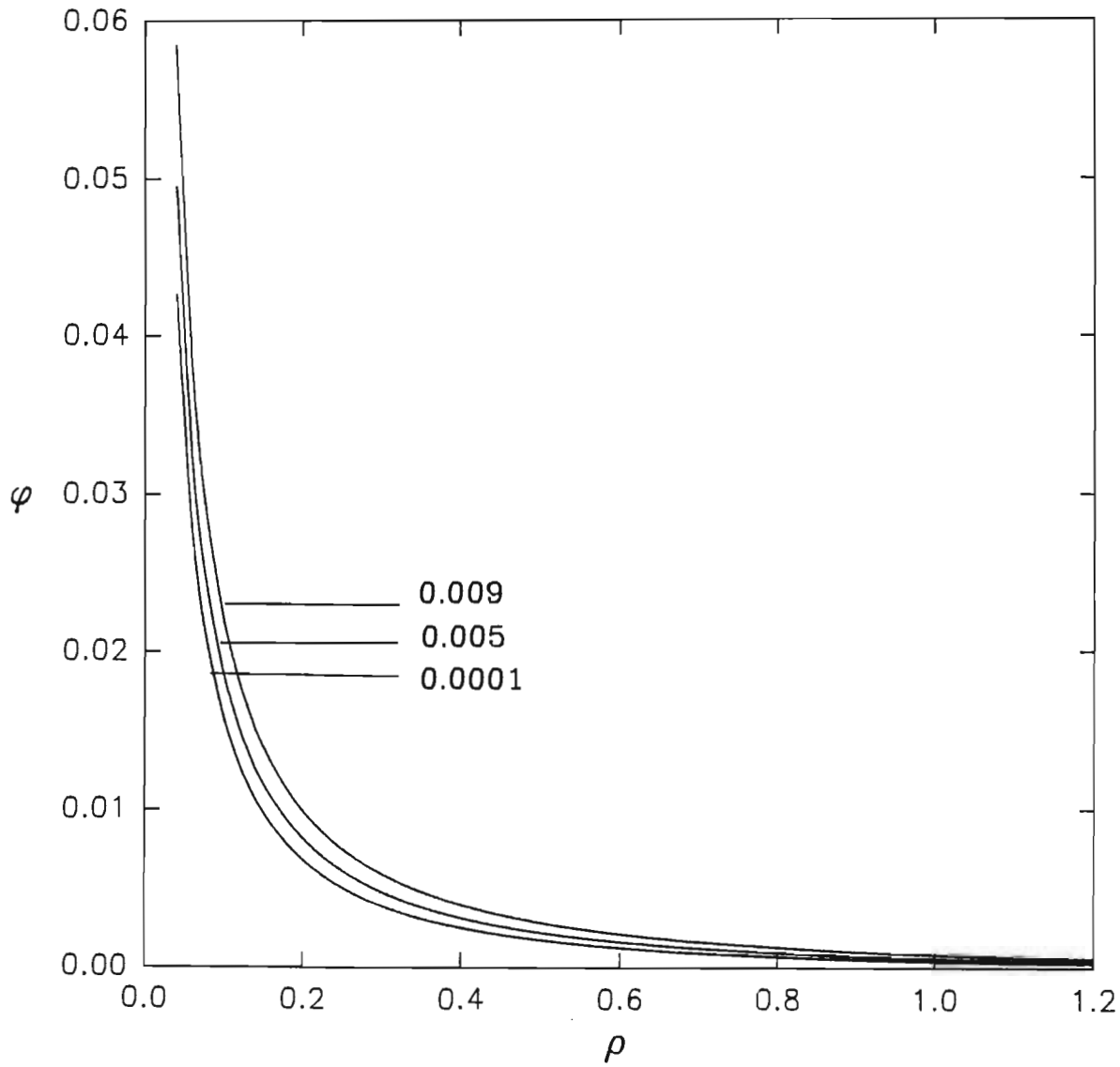

Figure 2.3: A numerical solution of the complete equation (2.10) for $T_e/T_i = 1$. The parameter labelling the curves is the normalized dust grain density n_{do}/n_o.

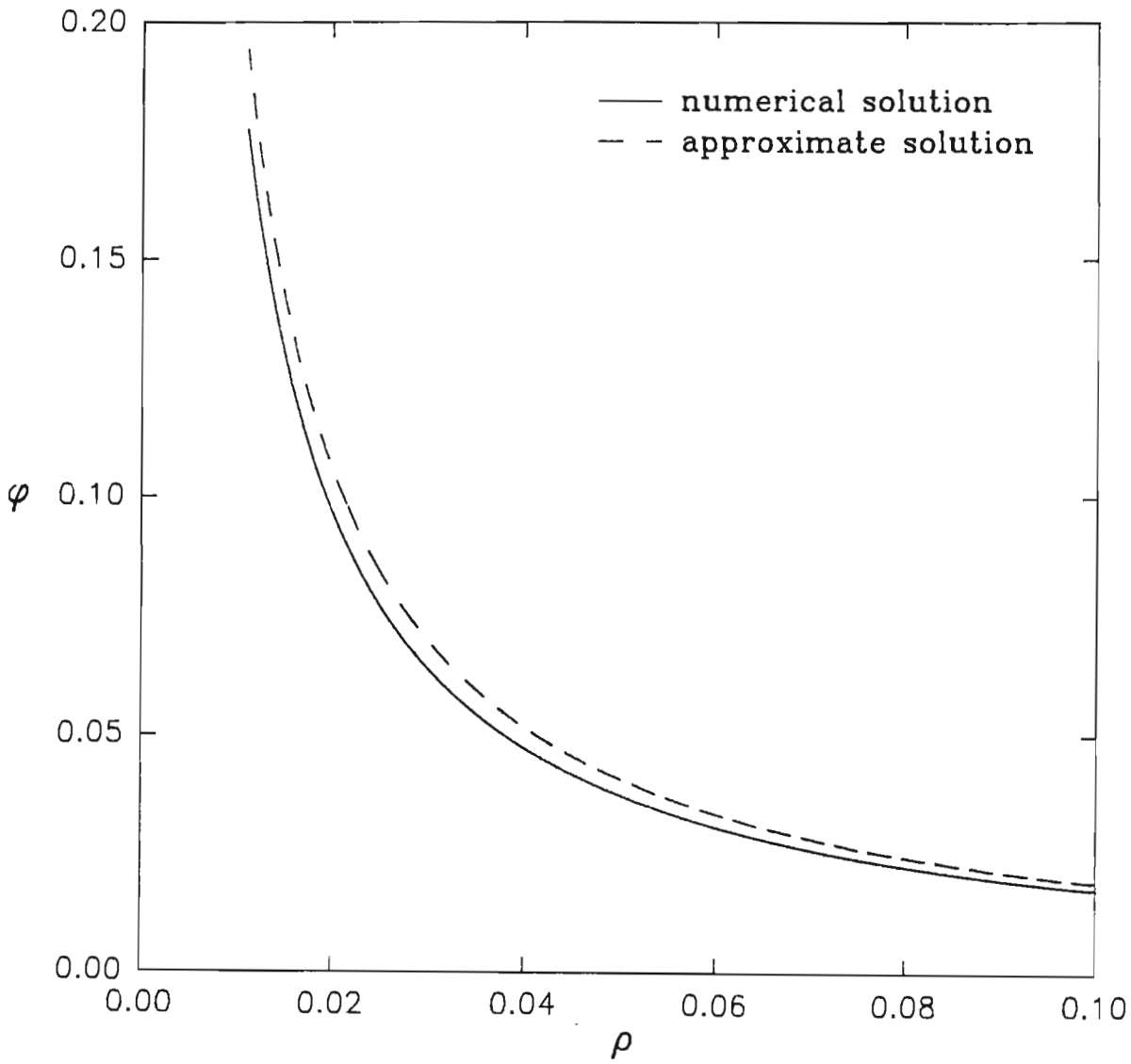

Figure 2.4: A comparison between the approximate solution (2.9) and a numerical solution of the complete equation (2.10) for $\mid e\phi/T_j \mid$ not too small. Here we fix $T_e/T_i = 1$ and $n_{do}/n_o = 0.005$.

numerically computed results are presented for $T_e/T_i = 1.0$. As the dust grain density increases (n_{eo}/n_o decreasing) the fall-off of ϕ is less rapid. This behaviour is consistent with the corresponding curve for the particular temperature ratio in Figure 2.1, where the effective Debye length is found to increase with n_{eo}/n_o decreasing. Finally, in Figure 2.4 we confirm the earlier results of Mak (1992) that the approximate solution (2.9) is a reasonable solution of the Poisson equation (2.5) even when the approximation $\mid e\phi/T_j \mid \ll 1$ is not strictly satisfied. The difference between the approximate analytical and numerical solutions at $\rho = 0.12$ is found to be 10%.

2.3 Summary

In this chapter we have examined the effect of Debye shielding in a dusty plasma in which the thermal electrons and ion have been taken as point particles having Boltzmann density distributions, while the massive, negatively charged dust grains are stationary. For small amplitude potentials, an analytical expression has been derived for the effective Debye length, which is found to be smaller than that in pure electron - ion plasma. The latter is found to decrease with the electron density for small values of T_e/T_i. On the other hand for $T_e/T_i \gg 1$, the electrons play little or no role in Debye shielding.

Next, an approximate analytical solution of the Poisson equation, using spherical coordinates, is compared with a numerical solution using a backward differencing scheme. The difference between the two solutions is found to be small in regions of parameter space where the approximations used in obtaining the approximate solution are valid. The effect of the electron density on the spatial decay of the potential, as obtained numerically, is found to be consistent with the approximate analytically

derived expression for the effective Debye length.

The results of this chapter have already been published in the journal Astrophysics and Space Science (S. Vidhya Lakshmi, R. Bharuthram and P.K. Shukla 1993).

Chapter 3

NONLINEAR POTENTIAL STRUCTURES IN A DUSTY PLASMA

3.1 Introduction

In a magnetized plasma Rossby-type wave (usually called drift-wave by plasma physicists) modes arise when there exists a gradient of the background magnetic field in a direction perpendicular to its line of action and the electric field perturbations are electrostatic in nature. Investigation on the properties of such waves, have been done originally by Rudakov and Sagdeev (1961) and more recently by others (e.g. Hasegawa and Mima 1978; Hasegawa, Maclennon and Kodama 1979) in connection with the spectrum cascade in drift-wave turbulence in magnetized plasmas, as well as by other authors (Makino, Kamimura and Taniuti 1981; Meiss and Horton 1983; Pavlenko and Petviashvili 1983) into nonlinear vortex-type solitons. Larichev and

Reznik (1976) were the first to produce a stationary nonlinear analytical solution in the form of dipolar vortices for the system of equations describing the evolution of 2-D Rossby waves.

Dust grains in a plasma can significantly modify the usual drift waves and also introduce a new type of drift mode. The latter is caused by the $\mathbf{E} \times \mathbf{B}$ motion of the negatively charged dust grains. These waves are similar to the impurity-ion drift waves (Ong and Yu, 1971). Dipolar vortex structures can exist when the set of nonlinear equations that governs the dynamics of the modified convective cells are included. Nonlinear dipolar vortex potential structures have been studied for dust drift waves (Shukla et al 1991) and for an inhomogeneous dusty plasma with stationary dust grains and a sheared ion flow (Bharuthram and Shukla 1992c). In this chapter, fluid theory is used to investigate the formation of nonlinear potential structures in an inhomogeneous magnetized dusty plasma consisting of hot electrons, cold ions and dust grains, taking into account the dynamics of all species. The model is essentially that used by Shukla et al (1991), with the inclusion here of magnetic curvature effects. However, in addition to studying the existence of dipolar vortex solutions, as done by them, we point out the existence of modified convective cell vortices in the complementary region of parameter space.

3.2 Basic Equations

Our model consists of a collisionless, magnetized non-uniform plasma in which the electrons have a temperature T_e, while the singly charged positive ions and the

negatively-charged, massive, dust grains are cold. Thus, in equilibrium the quasi-neutral condition reads

$$n_{io}(x) = n_{eo}(x) + Z_d n_{do}(x) \tag{3.1}$$

where $n_{jo}(x)$ is the equilibrium density of the j^{th} species ($j = d, e, i$) and $-Z_d e$ is the equilibrium charge of the dust particles.

The hot electrons are assumed to be in thermodynamic equilibrium. Their density is then given by the Boltzmann distribution,

$$n_e = n_{eo} \exp\left(\frac{e\phi}{T_e}\right) \tag{3.2}$$

where ϕ is the electrostatic potential and e is the magnitude of the electron charge.

The dynamics of the cold ion and dust fluids are governed by their continuity equation,

$$\partial_t n_j + \nabla \cdot (n_j \vec{v}_j) = 0 \qquad (j = i, d) \tag{3.3}$$

and the respective momentum equations,

$$\partial_t \vec{v}_i + \vec{v}_i \cdot \nabla \vec{v}_i = \frac{e}{m_i}\left[\vec{E} + \frac{1}{c}(\vec{v}_i \times \vec{B}_o)\right] \tag{3.4}$$

for the ions, and

$$\partial_t \vec{v}_d + \vec{v}_d \cdot \nabla \vec{v}_d = \frac{-Z_d e}{m_d}\left[\vec{E} + \frac{1}{c}(\vec{v}_d \times \vec{B}_o)\right] \tag{3.5}$$

for the dust grains. The external magnetic fields $\vec{B}_o = B_o(x)\hat{\mathbf{z}}$ is in the z-direction.

For $\partial_t \ll \Omega_j$, where $\Omega_j = \frac{|q_j|B_o}{m_j c}$ is the gyrofrequency of the j^{th} species ($j = i, d$), we have

$$\vec{v}_j = \vec{v}_E + \vec{v}_{Dj} + \vec{v}_{pj} + v_{zj}\hat{\mathbf{z}} \qquad (j = i, d)\,, \tag{3.6}$$

where

$$\vec{v}_E = \frac{c}{B_o}\hat{\mathbf{z}} \times \nabla\phi\,, \tag{3.7}$$

$$\vec{v}_{Dj} = \frac{c\mu_j \hat{\mathbf{z}} \times \nabla(\ln B)}{q_j} \approx -\frac{c\mu_j \hat{\mathbf{y}}}{q_j R}\,, \tag{3.8}$$

and

$$\vec{v}_{pj} = -\left(\frac{\epsilon_j c}{B_o \Omega_j}\right)[\partial_t + (\vec{v}_E + \vec{v}_{Dj} + v_{zj}\hat{\mathbf{z}}).\nabla]\nabla_\perp \phi \tag{3.9}$$

are the $\vec{E}\times\vec{B}$, curvature and polarization drifts respectively. Here $R^{-1} = -\nabla(\ln B)$ is the magnetic curvature, μ_j is the magnetic moment (taken to be constant) and $\epsilon_j = +1(-1)$ for $j = i,(d)$. It is noted that the gyrofrequency of the dust grains is given by $\Omega_d = \frac{Z_d e B_o}{m_d c}$.

Substituting equations (3.7) - (3.9) into (3.3) for the ion and dust fluids, we use the quasineutrality condition to obtain

$$\begin{aligned} &\frac{e}{T_e}\partial_t\phi - \frac{c}{B_o}\left(\frac{1}{R} + \kappa_n\right)\partial_y\phi + \partial_z v_{zi} + Z_d\frac{n_{do}}{n_{eo}}\partial_z(v_{zi} - v_{zd}) \\ &- \left[Z_d\frac{n_{do}}{n_{eo}}\frac{c}{B_o\Omega_d} + \frac{n_{io}}{n_{eo}}\frac{c}{B_o\Omega_i}\right]\left[\partial_t + \frac{c}{B_o}\hat{\mathbf{z}}\times\nabla\phi\cdot\nabla\right]\nabla_\perp^2\phi = 0\,, \end{aligned} \tag{3.10}$$

where $\kappa_n = \partial_x(\ln n_{eo}(x))$. In arriving at (3.10) we have assumed $v_E \cdot \nabla \gg v_{zj}\partial_z$.

The parallel (to $\vec{B}_o$) components of the ion and dust momentum equations (3.4) and (3.5) yield, respectively

$$\partial_t v_{zi} + \frac{c}{B_o}\hat{\mathbf{z}}\times\nabla\phi\cdot\nabla v_{zi} = -\frac{e}{m_i}\partial_z\phi\,, \tag{3.11}$$

and

$$\partial_t v_{zd} + \frac{c}{B_o}\hat{\mathbf{z}}\times\nabla\phi\cdot\nabla v_{zd} = \frac{Z_d e}{m_d}\partial_z\phi. \tag{3.12}$$

The set of equations (3.10) - (3.12) describe the nonlinear evolution of our system. However, before proceeding to a nonlinear analysis, we briefly examine the linear behaviour of the system. Upon linearizing (3.10) - (3.12) for perturbations varying as $\exp i(\vec{k}\cdot\vec{r} - \omega t)$, we obtain the local dispersion relation (Shukla et al 1991)

$$(1 + Z_d\delta_d k_\perp^2\rho_{sd}^2 + \delta_i k_\perp^2\rho_s^2)\omega^2 + \omega_*\omega - k_z^2(\delta_i C_s^2 + \delta_d Z_d C_{sd}^2) = 0\,. \tag{3.13}$$

Here $\omega_* = \frac{cT_e}{eB_o}k_y(\frac{1}{R} + \kappa_n)$, $\delta_d = Z_d(n_{do}/n_{eo})$ and $\delta_i = n_{io}/n_{eo}$, $\rho_s = C_s/\Omega_i$, $\rho_{sd} = C_{sd}/\Omega_d$, where $C_s = (T_e/m_i)^{\frac{1}{2}}$ is the ion acoustic speed and $C_{sd} = (T_e/m_d)^{\frac{1}{2}}$ is the dust acoustic speed. For $\delta_d = 0 (n_{do} = 0)$, we have the usual coupled ion acoustic - drift waves in an electron - ion plasma. On the other hand for the rare situation with no ions ($\delta_i = 0$), ie. a plasma with electrons and positively charged dust grains, the dispersion relation (3.13) reduces to that of coupled dust acoustic - drift waves. In its given general form, (3.13) describes the coupling between a hybrid acoustic wave with drift waves driven by the electron density gradient and the magnetic curvature effect.

3.3 Nonlinear Analysis

We consider stationary solutions of the equations (3.10) - (3.12) in the moving frame (x, ξ) where $\xi = y + \alpha z - Mt$, with α and M constant. Then (3.11), (3.12) and (3.10) become, respectively,

$$\left(-M\partial_\xi + \frac{c}{B_o}\hat{\mathbf{z}}\times\nabla\phi\cdot\nabla\right)v_{zi} = -\frac{e}{m_i}\alpha\partial_\xi\phi\,, \tag{3.14}$$

$$\left(-M\partial_\xi + \frac{c}{B_o}\hat{\mathbf{z}}\times\nabla\phi\cdot\nabla\right)v_{zd} = \frac{Z_d e}{m_d}\alpha\partial_\xi\phi\,, \tag{3.15}$$

and

$$\begin{aligned} &-\frac{Me}{T_e}\partial_\xi\phi - \frac{c}{B_o}\left(\frac{1}{R} + \kappa_n\right)\partial_\xi\phi + \alpha\partial_\xi v_{zi} + \delta_d\alpha\partial_\xi(v_{zi} - v_{zd}) \\ &-\frac{c}{B_o}\left(\frac{\delta_d}{\Omega_d} + \frac{\delta_i}{\Omega_i}\right)\left[-M\partial_\xi + \frac{c}{B_o}(z\times\nabla\phi\cdot\nabla)\right]\nabla_\perp^2\phi = 0\,. \end{aligned} \tag{3.16}$$

It is seen that (3.14) is satisfied by

$$v_{zi} = \frac{e\alpha}{Mm_i}\phi\,, \tag{3.17}$$

while

$$v_{zd} = -\frac{Z_d e\alpha}{M m_d}\phi \tag{3.18}$$

satisfies (3.15).

Inserting (3.17) and (3.18) into (3.16), we obtain

$$\left[-\frac{Me}{T_e} - \frac{c}{B_o}\left(\frac{1}{R} + \kappa_n\right) + \frac{e\alpha^2}{M m_i} + \delta_d \frac{\alpha^2 e}{M}\left(\frac{1}{m_i} + \frac{Z_d}{m_d}\right)\right]\partial_\xi \phi \tag{3.19}$$
$$-\frac{c}{B_o}\left(\frac{\delta_d}{\Omega_d} + \frac{\delta_i}{\Omega_i}\right)\left[-M\partial_\xi + \frac{c}{B_o}(z\times\nabla\phi\cdot\nabla)\right]\nabla_\perp^2\phi = 0\,.$$

The equation (3.20) is solved by letting

$$\nabla_\perp^2 \phi = C_1\phi + C_2\, x\,, \tag{3.20}$$

provided the constants C_1 and C_2 satisfy

$$\beta + \frac{c}{B_o}\left(\frac{\delta_d}{\Omega_d} + \frac{\delta_i}{\Omega_i}\right)\left[M\, C_1 + \frac{c}{B_o}\, C_2\right] = 0\,, \tag{3.21}$$

where

$$\beta = -\frac{Me}{T_e} - \frac{c}{B_o}\left(\frac{1}{R} + \kappa_n\right) + \frac{e\alpha^2}{M}\left[\frac{1}{m_i} + \delta_d\left(\frac{1}{m_i} + \frac{Z_d}{m_d}\right)\right]\,. \tag{3.22}$$

Solitary dipole vortex solutions of (3.20) can be constructed following standard methods (Larichev & Reznik 1976; Makino, Kamimura & Taniuti 1981; Meiss & Horton 1983; Shukla et al. 1991). Accordingly, we introduce the polar co-ordinates

$$r = (x^2 + \xi^2)^{1/2} \quad , \qquad \theta = tan^{-1}\,(\xi/x) \quad ,$$

and divide the (r, θ) plane into an inner region $r \leq R$ (where R is the vortex radius), and an outer region $r > R$.

In the outer region we prescribe rapidly decaying solutions for localization. Thus we set $C_2^o = 0$. From (3.21) we then find

$$C_1^o = \frac{-\beta}{M\frac{c}{B_o}\left(\frac{\delta_d}{\Omega_d} + \frac{\delta_i}{\Omega_i}\right)} \equiv a^2\,, \tag{3.23}$$

where the superscript ' o ' denotes the outer region. The outer solutions are given by

$$\phi_o = A^o K_1(ar)\cos\theta, \tag{3.24}$$

where A^o is a constant and K_1 is the modified Bessel function of the first order.

Since, for large r, the asymptotic form of $K_1(ar)$ is

$$r^{-\frac{1}{2}}\, exp(-ar),$$

localization is ensured provided $a > 0$, which yields (using (3.23))

$$M^2 + XM - \alpha^2 Y > 0\,, \tag{3.25}$$

where $X = \rho_{sd} C_{sd}\left(\frac{1}{R} + \kappa_n\right)$ and $Y = (\frac{m_d}{m_i})C_{sd}^2\left[1 + \delta_d\left(1 + Z_d\frac{m_i}{m_d}\right)\right]$.

The inner solution is

$$\phi^i = \left\{A^i J_1(br) + \left(\frac{C_2^i}{b^2}\right) r\right\}\cos\theta \tag{3.26}$$

where $b^2 = -C_1^i$, A^i is a constant, and J_1 is the Bessel function of the first kind. The superscript ' i ' denotes the inner region. The constants C_1^i and C_2^i satisfy (3.21).

Continuity of ϕ, $\partial_r\phi$ and $\bigtriangledown^2\phi$ at $r = R$, yield

$$A^o = \frac{C_2^i R}{\{(a^2 + b^2)K_1(aR)\}}\,, \tag{3.27}$$

$$A^i = -\frac{C_2^i R a^2}{\{b^2(a^2 + b^2)J_1(bR)\}}\,, \tag{3.28}$$

and

$$\frac{K_2(aR)}{aK_1(aR)} = -\frac{J_2(bR)}{bJ_1(bR)}. \tag{3.29}$$

For a given a, which depends on M, α and the plasma parameters, (3.29) yields the value of b. Then using (3.21), (3.28) and (3.28), the dipole vortex structure is completely determined. As mentioned, the existence of the dipole-vortex solutions requires $a^2 \equiv C_1^o > 0$, which reduces to (3.25). The existence region for such solitary dipole-vortices is shown by the shaded region in Figure 3.1. Here we have used the following fixed parameters: $\rho_{sd}/R = \rho_{sd}\kappa_n = 0.01$, $Z_d = 100$, $n_{d0}/n_{i0} = 0.005$ and $m_d = 1000\, m_i$.

In the un-shaded region of Figure 3.1, $C_1^o < 0$. We examine the nature of the outer solutions when this inequality holds. We write $C_1^o = -\tilde{C}_1^o$, where $a^2 = \tilde{C}_1^o > 0$. Then proceeding as above, the outer solution is found to be given by, using ψ to now represent the potential,

$$\psi^o = D^o Y_1(ar)\cos\theta\,, \tag{3.30}$$

where D^o is a constant, and Y_1 is the modified Bessel function of the second kind. The inner solution is , once again, given by (3.26), with $b^2 = C_1^i$. We write it as,

$$\psi^i = \left\{ D^i J_1(br) + \left(\frac{C_2^i}{b^2}\right) r \right\} \cos\theta\,. \tag{3.31}$$

The continuity of ψ, $\partial_r\psi$ and $\nabla^2\psi$ at $r = R$, yield

$$D^o = \frac{C_2^i R}{\{(b^2 - a^2)Y_1(bR)\}}, \tag{3.32}$$

$$D^i = \frac{C_2^i R a^2}{\{b^2(b^2 - a^2)J_1(bR)\}}, \tag{3.33}$$

and

$$\frac{Y_2(aR)}{aY_1(aR)} = \frac{J_2(bR)}{bJ_1(bR)}. \tag{3.34}$$

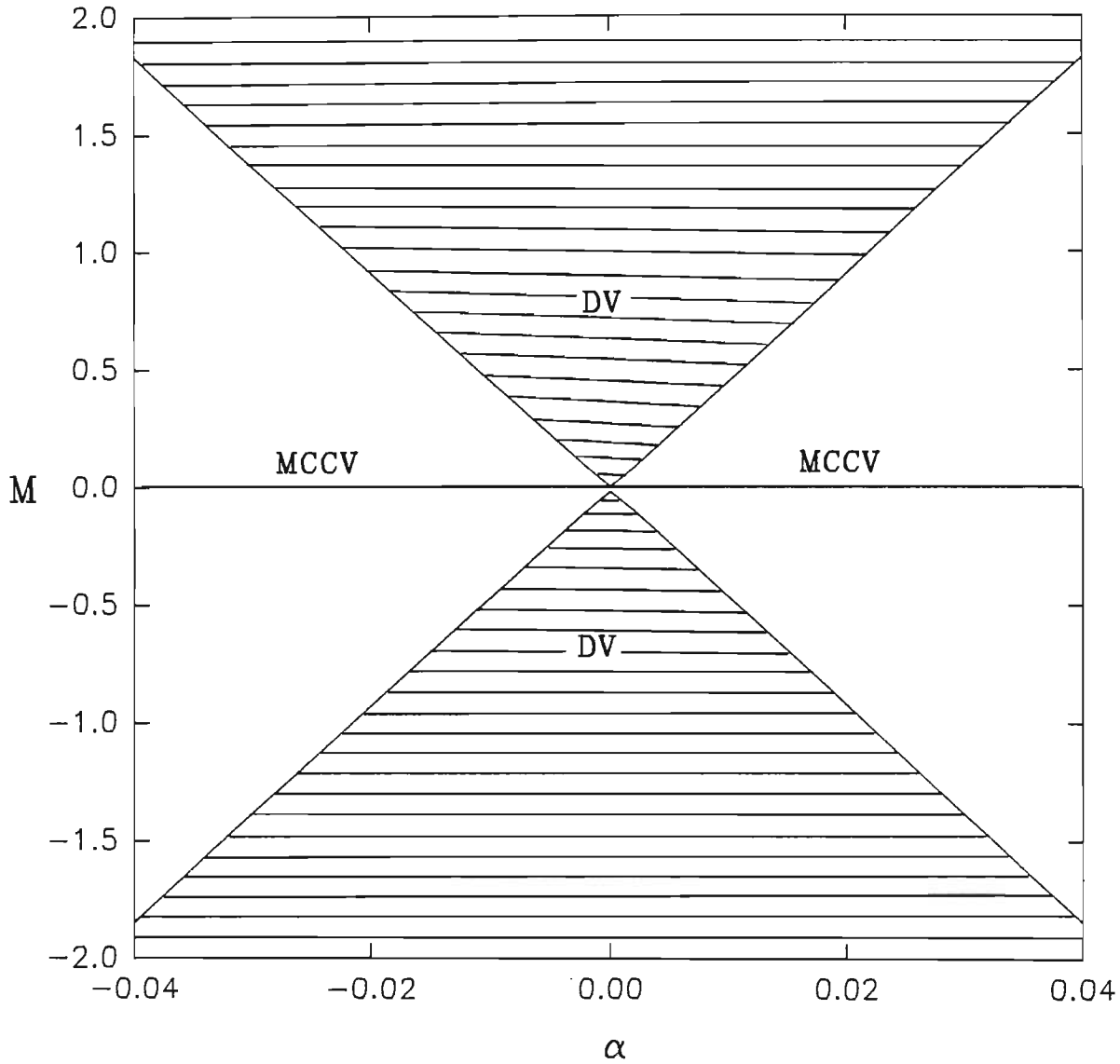

Figure 3.1: Diploar vortices (DV) and modified convective cell vortices (MCCV) can exist in the regions indicated in the parameter space (M, α).

As pointed out by Shukla and Yu (1984), the latter solutions ((3.30) - (3.34)) represent modified convective cell motion. Convective cells are associated with fluid vortex motion, due to the $\mathbf{E} \times \mathbf{B_o}$ drift of the ions and electrons. This can cause Bohm-like diffusion even in an equilibrium plasma. The convective cell and the related motion on plasma transport has been studied (Okuda and Dawson 1973; Hasegawa and Mima 1977, 1978; Hasegawa, MacLennon and Kodama 1979). Okuda and Dawson (1973) in their study of three dimensional effects on the convective cell motion, found that by introducing a small $k_{\|}(k_{\|}^2/k^2 \ll m/M, k_{\|}v_{te} \ll \omega, v_{te}$ is the electron thermal velocity) the convective cells attain a real frequency $\omega_r = (k_{\|}/k)(M/m)^{\frac{1}{2}}\Omega_i$, where $\omega_r \ll \Omega_i$. Here, m and M are the mass of the electron and ion respectively, and $\Omega_i = eB_o/Mc$ is the gyrofrequency. In our studies, the convective cell motion is due to the $\mathbf{E} \times \mathbf{B}$ motion of the dust grains.

In this case, the outer solution (3.30) (for $r > R$) oscillates about zero with the envelope of the oscillation decreasing slowly in the radial direction. This solution is less localized than the dipole vortex solution (3.24) which decreases monotonically as $r \to \infty$. It is interesting to note that these two types of solutions exist in complementary regions of the parameter space reflected in Figure 3.1.

3.4 Conclusion

We have examined the existence of nonlinear potential structures in an homogeneous, magnetized dusty plasma in which the hot electrons have a Boltzmann density distribution, while the cold ions and dust grains are represented by the fluid equations. The model is essentially that of Shukla et al.(1991). The set of nonlinear equations describing the evolution of the system has been derived. In the linear limit, it is shown

to produce a dispersion relation for coupled hybrid acoustic - drift waves, where the frequency of the hybrid acoustic wave is determined by the ion acoustic and dust acoustic frequencies.

Stationary solutions of the system of nonlinear equations yield dipolar vortex potential structures and less localized oscillatory solutions in complementary regions of parameter space (Figure 3.1).

The localized potential structures discussed in this paper may be responsible for enhanced particle and heat transport (in dusty plasmas in space, as well as laboratory plasmas). In particular, an ensemble of such randomly distributed structures can constitute a new turbulent state. Their associated electromagnetic fields can enhance transport across confining magnetic fields. Furthermore, the presence of the massive dust grains introduces a new range of low frequencies for fluctuation phenomena.

The results of this chapter have already been published in the journal Astrophysics and Space Science (S. Vidhya Lakshmi, R. Bharuthram and M. Y. Yu 1993).

Chapter 4

ARBITRARY AMPLITUDE DUST-ACOUSTIC SOLITONS

4.1 Introduction

Our investigations in this chapter are on the existence of large amplitude rarefactive and compressive dust-acoustic solitons in an unmagnetized four component plasma consisting of electrons, two distinct positive ion species of different temperatures and massive, negatively-charged, dust grains. Nonlinearity effects cause wave steepening leading to wave breaking. Dispersion, on the otherhand leads to a spreading of a travelling wave. When the two effects balance, a nonlinear wave packet called a soliton is produced. It has a pulse-like waveform. In addititon to laboratory experiments, solitons were observed in auroral plasma (Temerin et al. 1982, Mozer and Temerin 1983, Temerin and Mozer 1984) and in the magnetosphere (Boström et al. 1988). In our studies, the effects of the particle densities and temperatures on the soliton amplitude and Mach number are examined.

Dust-acoustic modes in dusty plasmas have been treated by number of authors. Rao et al. (1990) investigated the linear and weakly non-linear properties of dust-acoustic waves using a model in which they considered the dynamics of a tenuous dust fluid, with the electrons and ions assumed to be in electrostatic equilibrium, their number densities given by the Boltzmann distribution. They showed the existence of dust-acoustic waves and dust-acoustic solitons in unmagnetized dusty plasmas.

Bharuthram and Shukla (1992) employed a similar model, but incorporated both cool and hot Boltzmann-distributed ions to show the existence of dust-acoustic double layers in a dusty plasma. Their work was extended by Mace and Hellberg (1993), who included ion inertia effects. A review paper on double layers and solitons in dusty plasmas has been presented by Verheest (1993).

4.2 Theory

Our plasma model consists of Boltzmann-distributed electrons, two distinct groups of thermal positive ions, their densities given by Boltzmann distributions with different temperatures, and a negatively-charged, cold dust fluid whose dynamics are governed by the continuity and momentum equations. It is exactly the model used by Bharuthram and Shukla (1992) in an investigation of double layer potential structures.

The basic equations derived below have been obtained by Bharuthram and Shukla (1992). For purposes of completeness we present them in some details. We consider a collisionless, unmagnetized plasma consisting of electrons having a temperature T_e, two distinct groups of warm ions having temperatures T_c (for the cool species) and T_h

(for the hot species) and negatively-charged, extremely heavy, dust particles. Thus, in equilibrium the quasi-neutrality condition reads

$$n_{co} + n_{ho} = n_{eo} + Z_d n_{do}\,, \tag{4.1}$$

where n_{jo} is the equilibrium density of the j^{th} species ($j = e, c, h$) and $n_{do}(-Z_d e)$ is the equilibrium density (charge) of the dust particles. The number densities of the electron and ion fluids are given by their respective Boltzmann distributions, viz,

$$n_e = N_{eo}\, exp(\alpha_e \phi)\,, \tag{4.2}$$

$$n_c = N_{co}\, exp(-\alpha_c \phi)\,, \tag{4.3}$$

and

$$n_h = N_{ho}\, exp(-\alpha_h \phi)\,, \tag{4.4}$$

where $\alpha_j = T_{eff}/Z_d T_j$, $\phi = Z_d e\Phi/T_{eff}$, the effective temperature T_{eff} is defined by (Bharuthram and Shukla, 1992) $Z_d^2 n_{do}/T_{eff} = n_{eo}/T_e + n_{co}/T_c + n_{ho}/T_h$, Φ is the electrostatic potential and densities have been normalised by the "effective" density $Z_d n_{do}$ of the dust particles. Thus $n_j = n'_j/Z_d n_{do}$ and $N_{jo} = n_{jo}/Z_d n_{do}$ where $n'_j = n_{jo}\, exp(\pm\alpha_j \phi)$ is the actual density of the species j.

The dynamics of the cold dust grains are governed by continuity and momentum equations,

$$\partial_t n'_d + \partial_x (n'_d v_d) = 0\,, \tag{4.5}$$

and

$$(\partial_t + v_d \partial_x) v_d = \partial_x \phi\,, \tag{4.6}$$

where we have introduced $n'_d = Z_d n_d$. We close the system of equations with Poisson's equation,

$$\partial_x^2 \phi = n_e + n'_d - n_c - n_h. \tag{4.7}$$

Here we have normalised the dust fluid velocity v_d by the dust acoustic speed $C_{sd} = (T_{eff}/m_d)^{\frac{1}{2}}$, the spatial length by the dust Debye length $\lambda Dd = C_{sd}/\omega_{pd}$ and the time is in units of the inverse dust plasma frequency $\omega_{pd}^{-1} = (m_d/4\pi n_{do} Z_d^2 e^2)^{\frac{1}{2}}$. For perturbations varying as $exp\{i(kx - \omega t)\}$, where k is the wavenumber and ω the frequency, linearization of the equations (4.3) - (4.7) yields $\omega = kC_{sd}/(1 + k^2\lambda Dd^2)^{\frac{1}{2}}$, which is the dispersion relation for dust-acoustic waves (Rao et al, 1990).

We now look for solutions of equations (4.5) - (4.7) in the stationary frame $\xi = x - Mt$ where $M(= V/C_{sd})$ is the Mach number. Accordingly, from equations (4.5) and (4.6) one finds the normalised number density for dust particles as

$$n_d' = M/(M^2 + 2\phi)^{\frac{1}{2}}\,, \tag{4.8}$$

where the plasma is assumed to be unperturbed at $\mid \xi \mid \rightarrow \infty$ and we have used the appropriate boundary conditions $n_d' = 1, v_d = 0$ and $\phi = \partial_\xi \phi = 0$ at $\mid \xi \mid \rightarrow \infty$. Substituting for particle number densities from equations (4.2) - (4.4) and (4.8) into (4.7), multiplying both sides by $\partial_\xi \phi$ and integrating once with the chosen boundary conditions, we obtain

$$\frac{1}{2}(\partial_\xi \phi)^2 + \psi(\phi) = 0\,, \tag{4.9}$$

where the Sagdeev potential(Sagdeev, 1965) is given by

$$\begin{aligned}\psi(\phi) = \frac{N_{eo}}{\alpha_e}[1 - exp(\alpha_e \phi)] + [M^2 - M(M^2 + 2\phi)^{\frac{1}{2}}] + \\ \frac{N_{co}}{\alpha_c}[1 - exp(-\alpha_c \phi)] + \frac{N_{ho}}{\alpha_h}[1 - exp(-\alpha_h \phi)]\,.\end{aligned} \tag{4.10}$$

For the existence of soliton potential structures one requires (Sagdeev, 1965) that

(i) $\psi(\phi) = \partial_\phi \psi(\phi) = 0$ at $\phi = 0$,

(ii) $\psi(\phi) = 0$ at some $\phi = \phi_m$ and $\partial_\phi \psi(\phi_m) < (>) 0$ for

$\phi_m < (>)0$,

(iii) $\psi(\phi) < 0$ for $0 <| \phi |<| \phi_m |$.

For ion-acoustic phenomena in ordinary electron-ion plasmas (moving positively-charged heavier ions and Boltzmann negatively-charged electrons) such solitons are referred to as compressive solitons (Baboolal et al, 1990). However, as pointed out by Verheest (1993), in our model of a dusty plasma with negatively-charged dust particles the role of the charged particles are reversed (moving negatively-charged massive dust grains, Boltzmann positively-charged ions). Hence, here solitons with $\phi_m > 0$ are rarefactive and $\phi_m < 0$ are compressive in nature. This will be easier to see when the numerical solutions are presented.

4.3 Numerical solutions

4.3.1 Rarefactive solitons

Initially, we consider a plasma consisting solely of positive ions and negative dust particles, i.e. $N_{eo} = 0$, a cool to hot ion temperature ratio of $T_c/T_h = 0.05$ and a cool to hot ion density ratio of 0.1/0.9 and typical forms of the Sagdeev potential $\psi(\phi)$ for different values of M are computed. This is depicted in Figure 4.1. It is seen there exists a value of Mach number $M(M = 1.159)$ beyond which solitons do not exist. At the cut-off, the Sagdeev potential has a double humped structure ($\partial_\phi \psi = 0$ at $\phi = 0$ and $\phi = \phi_m$), corresponding to a double layer structure (Bharuthram and Shukla 1986, Baboolal et al 1988, 1990). This point will be discussed later. The soliton potential half-profiles corresponding to the curves in Figure 4.1 are shown in Figure 4.2. For such profiles it is seen from equation (4.8) that the dust density has a minimum value at $\xi = 0$, corresponding to a dip in density (rarefactive structure).

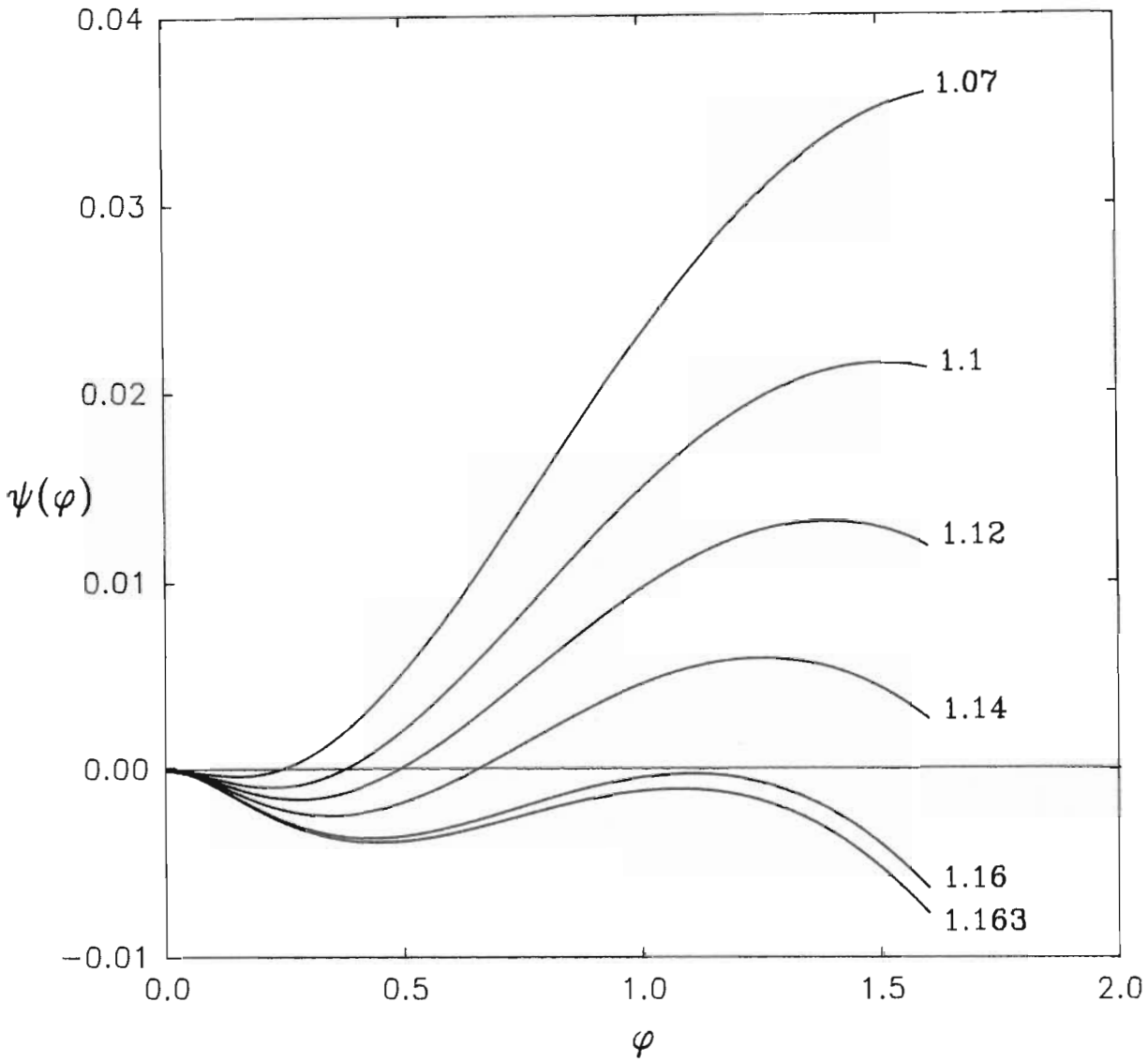

Figure 4.1: Typical forms of the large amplitude Sagdeev potential $\psi(\phi)$ for rarefactive solitons. The fixed plasma parameters are $N_{eo} = 0, T_c/T_h = 0.05$, and $N_{co}/N_{ho} = 0.1/0.9$. The parameter labelling the curves is the Mach number M.

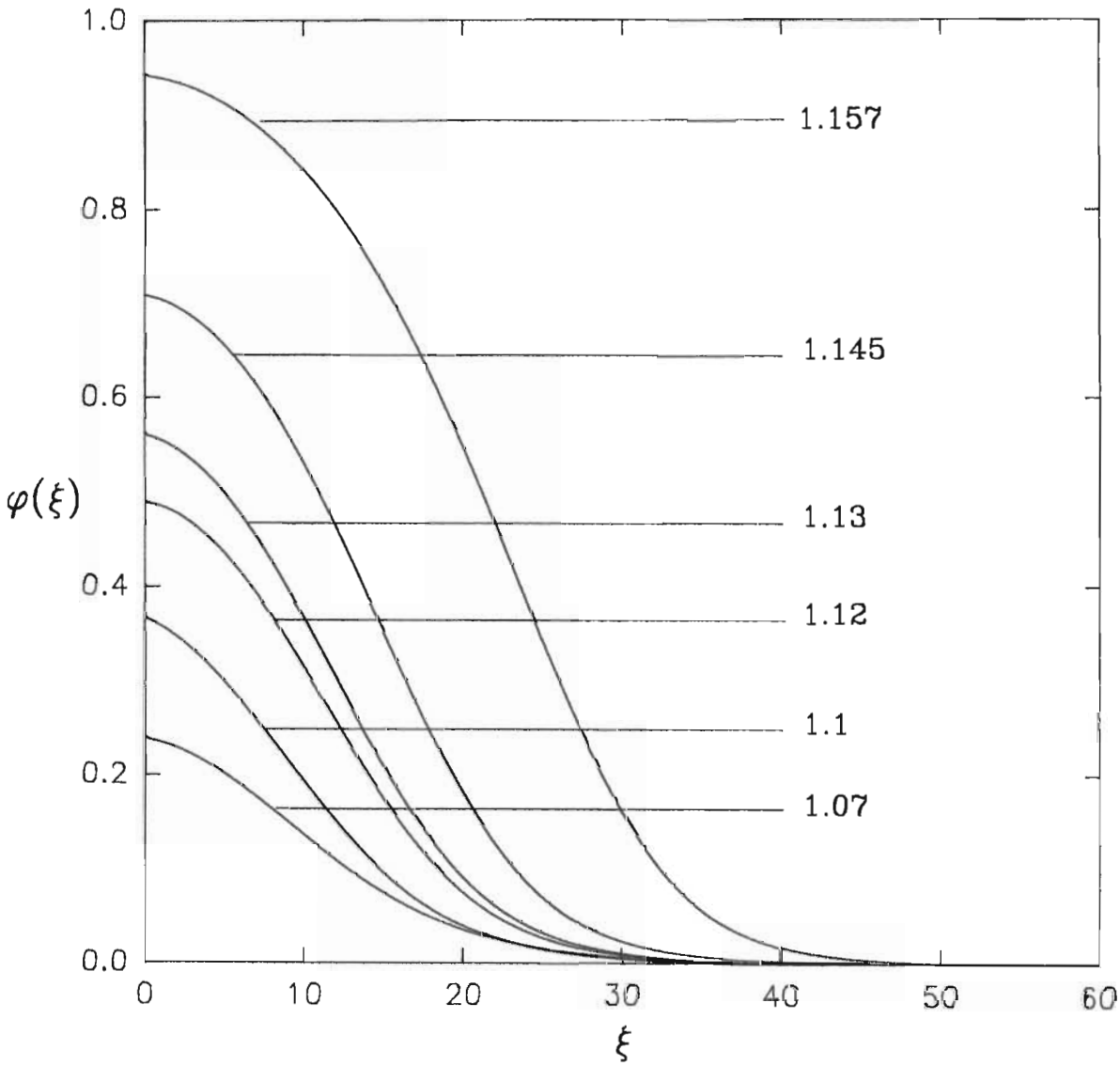

Figure 4.2: The soliton potential half-profiles corresponding to the curvesin Figure 4.1.

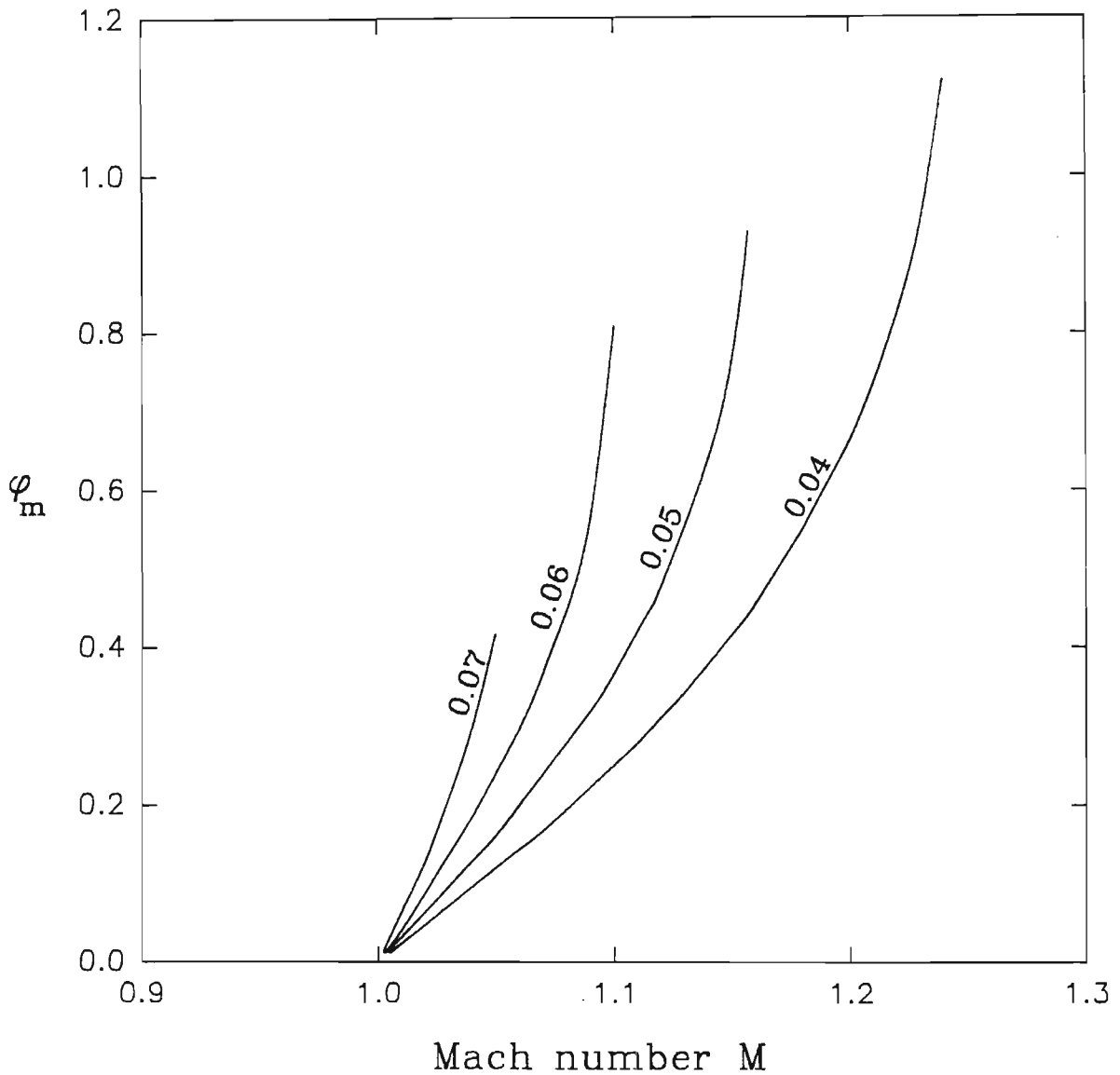

Figure 4.3: Variation of the soliton amplitude ϕ_m with the Mach number M. The parameter labelling the curves is the ratio of cool to hot ion temperature T_c/T_h. Other fixed parameters are as in Fig. 4.1.

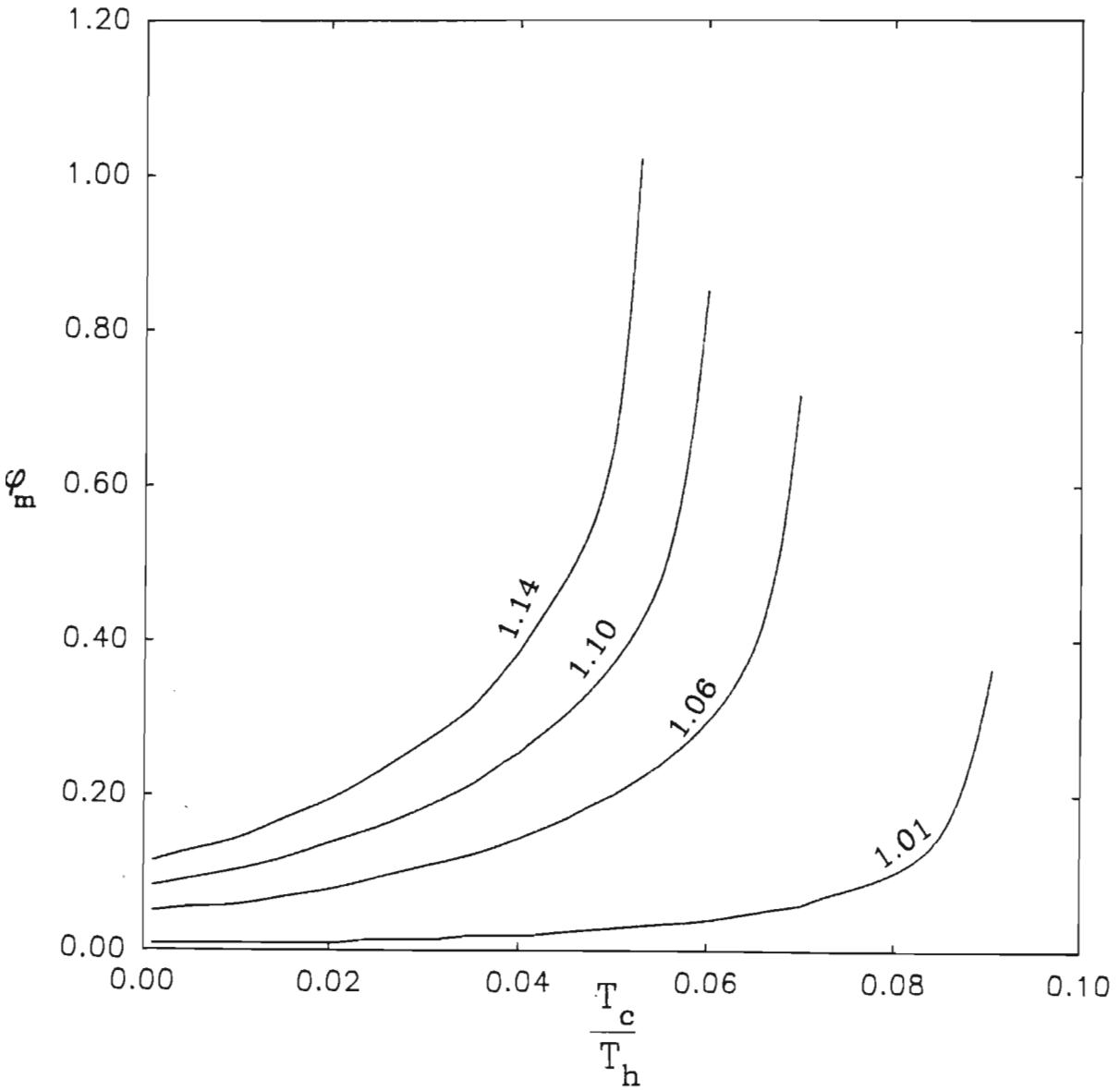

Figure 4.4: Variation of the soliton amplitude ϕ_m with the ratio of cool to hot ion temperature T_c/T_h. The parameter labelling the curves is the Mach number M. Other fixed parameters are as in Fig. 4.1.

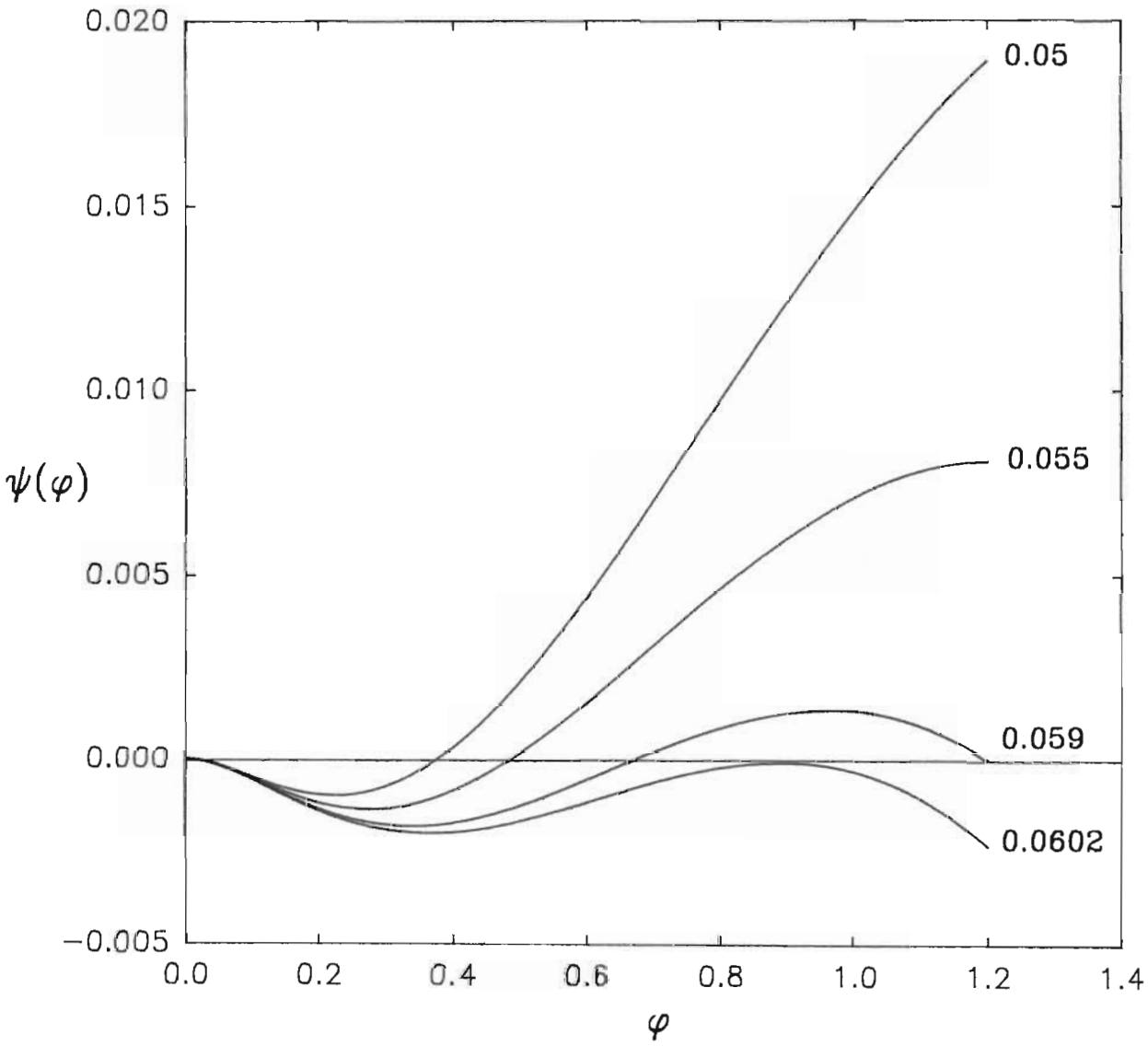

Figure 4.5: The typical forms of the Sagdeev potential for different values of T_c/T_h with $M = 1.1$. Other fixed parameters are as in Fig. 4.1.

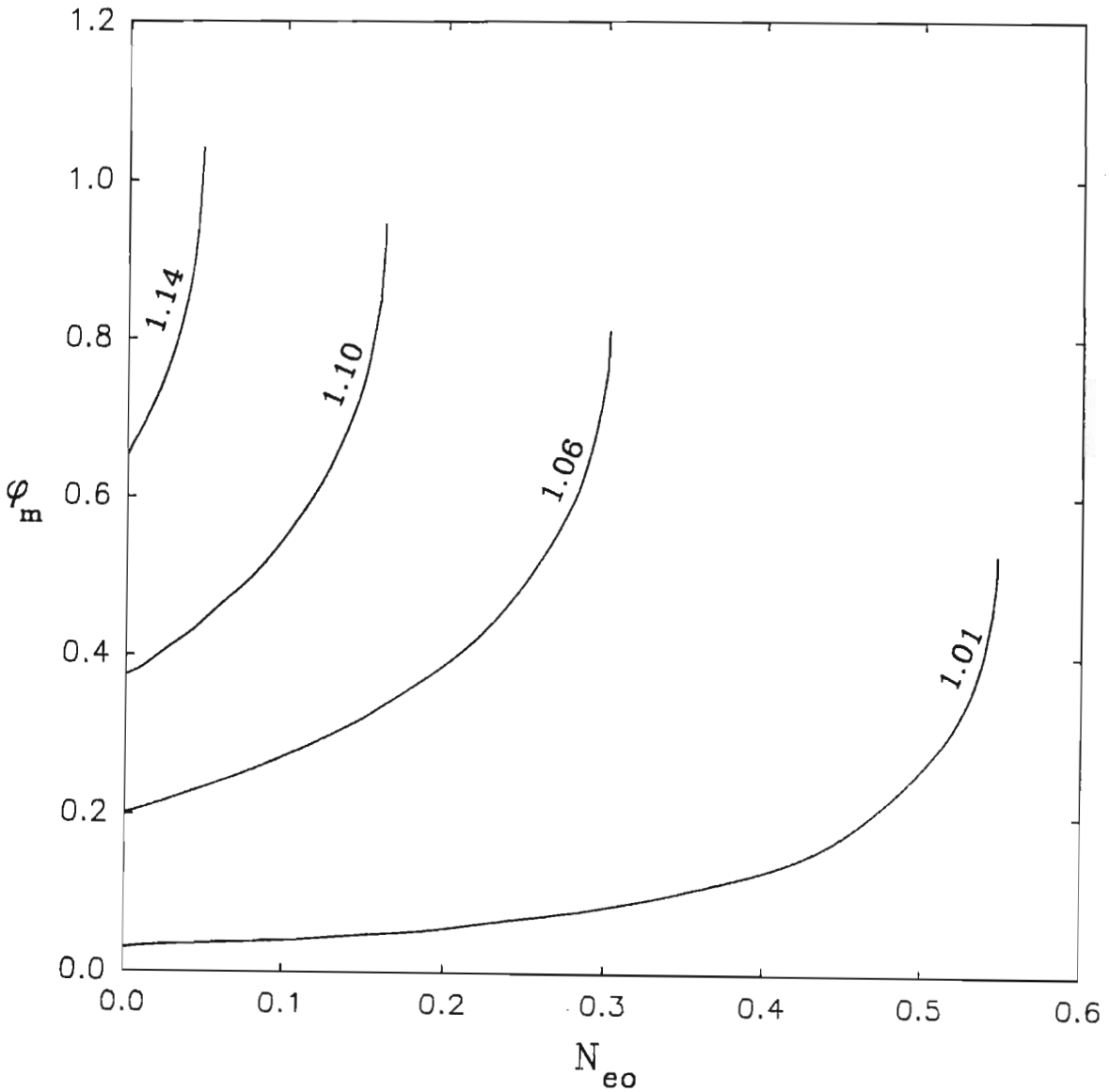

Figure 4.6: Variation of the soliton amplitude ϕ_m with the normalised electron density N_{eo}. The parameter labelling the curves is the Mach number M. Here $T_e/T_h = 10$, with the other fixed parameters are as in Fig. 4.1.

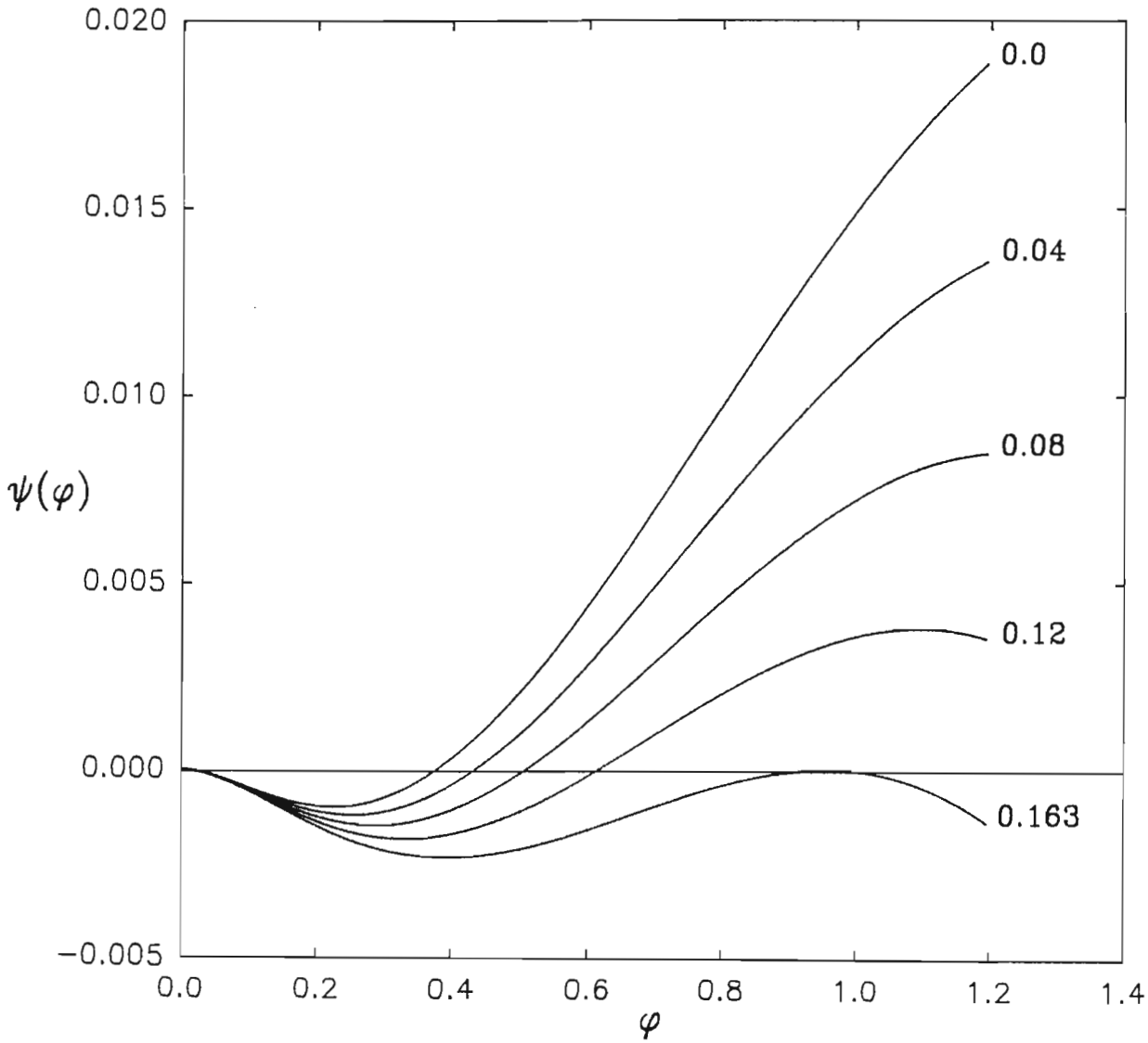

Figure 4.7: The typical forms of the Sagdeev potential $w(\phi)$ for different values of N_{eo} with $M = 1.1$. The other fixed parameters are as in Fig. 4.6.

The variation of ϕ_m with Mach number M, for fixed T_c/T_h, is shown in Figure 4.3. It is seen that only supersonic ($M > 1$) solitons are found to exist. Furthermore the range of M - values for soliton formation narrows sharply as T_c/T_h increases slightly.

The variation of the soliton amplitude ϕ_m with T_c/T_h is shown in Figure 4.4 for different M values. For each value of M, there exists an upper threshold of T_c/T_h beyond which no solitons occur, e.g. for M = 1.1 the limit is $T_c/T_h = 0.06$. This is clearly shown in Figure 4.5 where the formation of a double layer potential profile constitutes the boundary of soliton formation. Such double layer formation is attributed to an imbalance of the charge distribution caused by the two ion species, thus producing an isolated electric field within the plasma. Associated with this field is a double layer potential structure. It is seen from Figure 4.4 that as the value of M increases, solitons are found for a narrower range of T_c/T_h values.

Next we consider the effect of a finite electron population. Figure 4.6 shows the variation of ϕ_m with the normalised electron density N_{eo} for different values of M. The fixed parameters are $T_e/T_h = 10.0$ and $T_c/T_h = 0.05$. For a given Mach number we observe that as the electron density increases, the soliton amplitude also increases, with an upper limit of N_{eo} beyond which no solitons are found. The effect of N_{eo} on the Sagdeev potential for a fixed M value is shown in Figure 4.7

The increase in ϕ_m with N_{eo} may be explained as follows. A measure of the wave dispersion is given by the quantity $\Delta = \mid \frac{d\omega}{dk} \mid - \mid \frac{d^2\omega}{dk^2} \mid$ (Taniuti and Nishihara 1983). The smaller Δ, the larger the dispersion. It is found that $\Delta(N_{eo} = 0) > \Delta(N_{eo} = 0.1)$. Thus the dispersion is stronger when a finite electron population is present. This has to be balanced by a stronger nonlinearity for soliton formation, leading to an increase in soliton amplitude.

A study of the effect of the electron temperature on the soliton amplitude is shown in Figure 4.8 for a fixed $N_{eo} = 0.1$. As T_e/T_h decreases the soliton amplitude ϕ_m increases. However, at the critical value of $T_e/T_h = 1.74$, the Sagdeev potential becomes double layer in character, beyond which no solitons occur (in a manner similar to Figure 4.5). We illustrate in Figure 4.9, the dependence of the soliton amplitude on the cool to hot ion density ratio N_{co}/N_{ho} for different values of N_{eo}. The fixed parameters are $M = 1.1$, $T_c/T_h = 0.05$ and $T_e/T_h = 10$. We observe that the range of N_{co}/N_{ho} values over which solitons are possible is severely limited as N_{eo} increases.

Figure 4.10 presents the $N_{co}/N_{ho} - N_{eo}$ parameter space over which soliton formation is possible. The parameter labelling the boundary curves is T_c/T_h. Solitons occur within the area bounded by the curves and the N_{co}/N_{ho}-axis. For the chosen fixed parameters, no solitons are found for $T_c/T_h > 0.065$.

4.3.2 Compressive solitons

For the purpose of a comparative study, here also, we consider a plasma consisting solely of positive ions and negative dust particles (electron density N_{eo}=0), a cool to hot ion density ratio $N_{co}/N_{ho} = 0.2/0.8$ and a cool to hot ion temperature ratio of $T_c/T_h = 0.05$. Typical forms of the Sagdeev potential $\psi(\phi)$ for compressive solitons ($\phi_m < 0$) for different values of Mach number M are shown in Figure 4.11 with the associated compressive soliton profile shown in Figure 4.12 for $M = 1.05$. We find, that there exists a lower and an upper cut-off value of M, beyond which solitons do not exist. It is observed that at the upper cut-off the Sagdeev potential does not have a limiting double-humped structure corresponding to a double layer potential structure as found for the rarefactive solitons. We have shown in theory (eqbn(4.8))

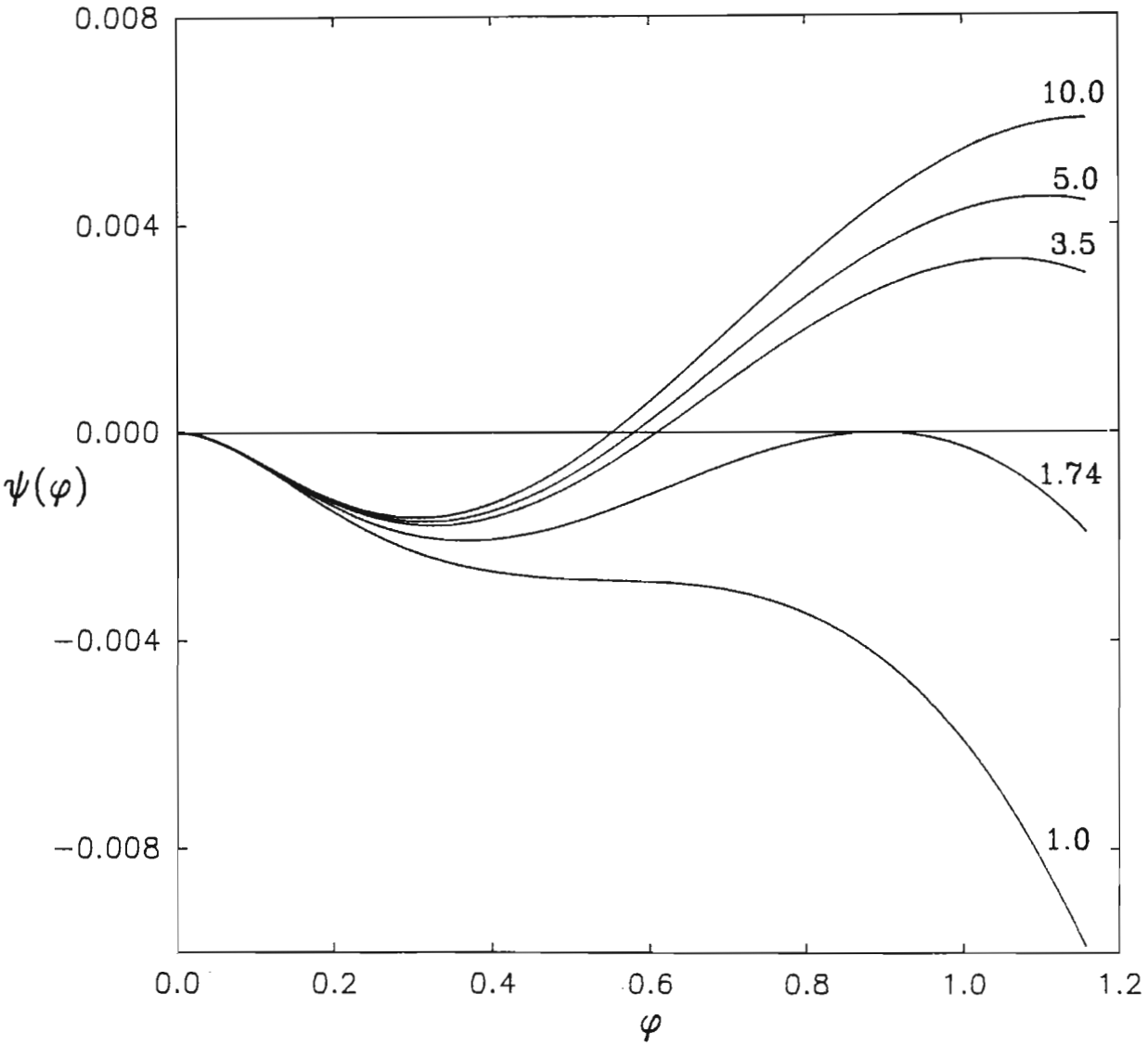

Figure 4.8: The Sagdeev potential $\psi(\varphi)$ for various ratios of electron to hot ion temperature T_e/T_h. The fixed parameters are $N_{eo} = 0.1$, $T_c/T_h = 0.05$ and $M = 1.1$.

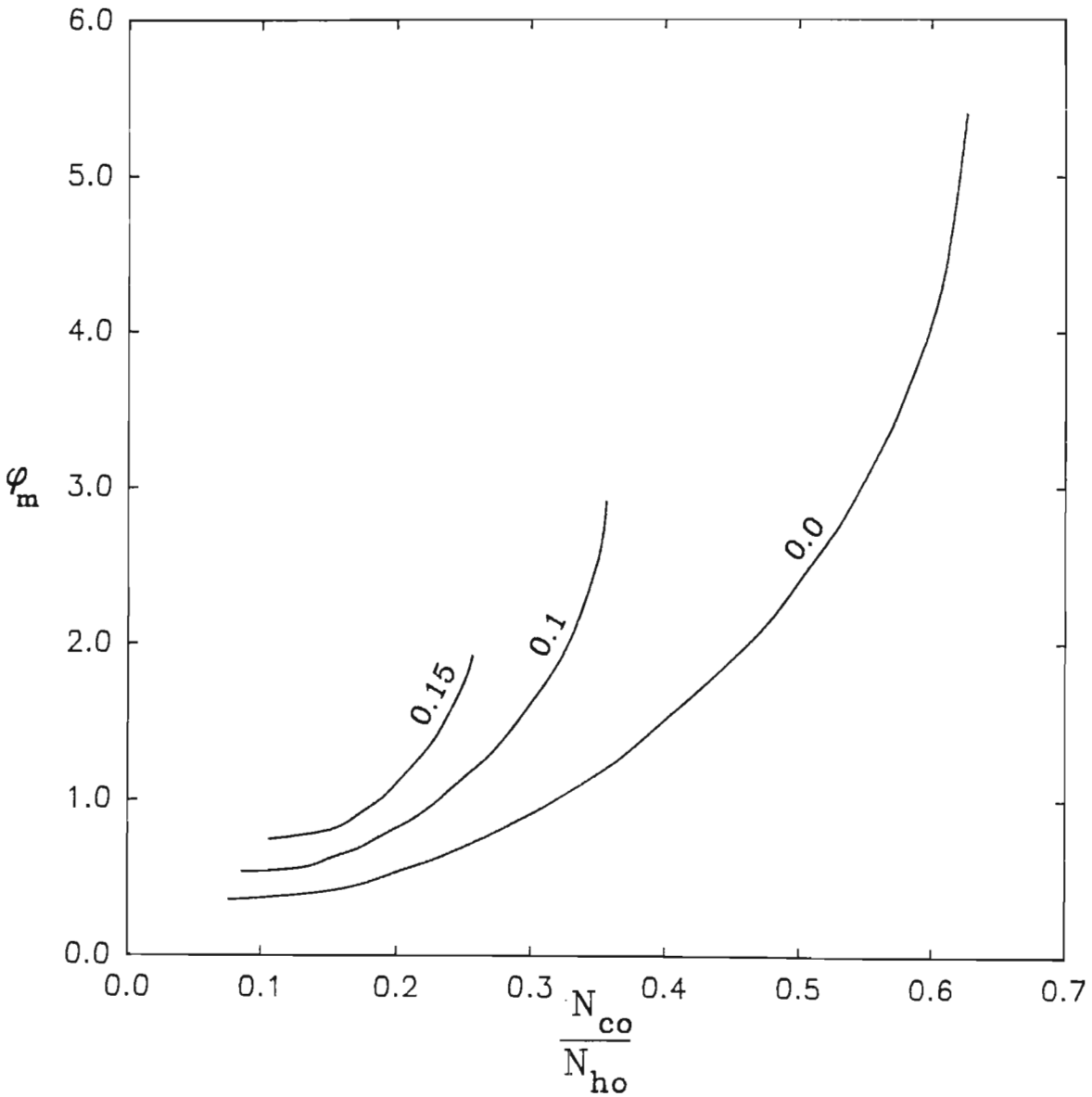

Figure 4.9: Variation of the soliton amplitude ϕ_m with the cool to hot ion density ratio N_{co}/N_{ho} for $T_e/T_h = 10$. The parameter labelling the curves is N_{eo}. The other fixed parameters are as in Figure 4.8.

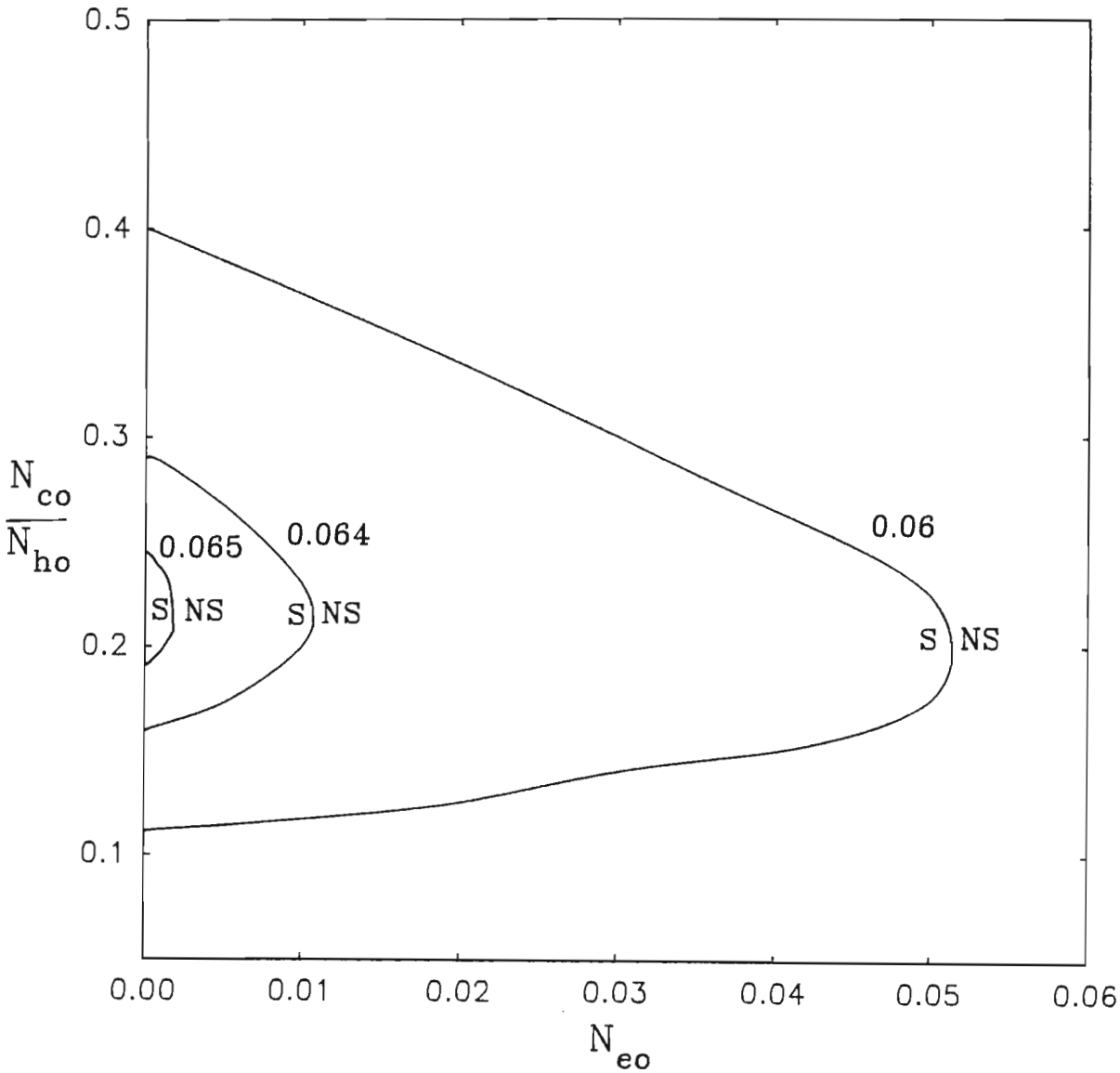

Figure 4.10: The existence region for soliton formation in the N_{co}/N_{ho} - N_{eo} space for different values of T_c/T_h. Solitons are found in the region bounded by the N_{co}/N_{ho} - axis and each curve (area labelled S). Beyond the curves no solitons are possible (area labelled NS).

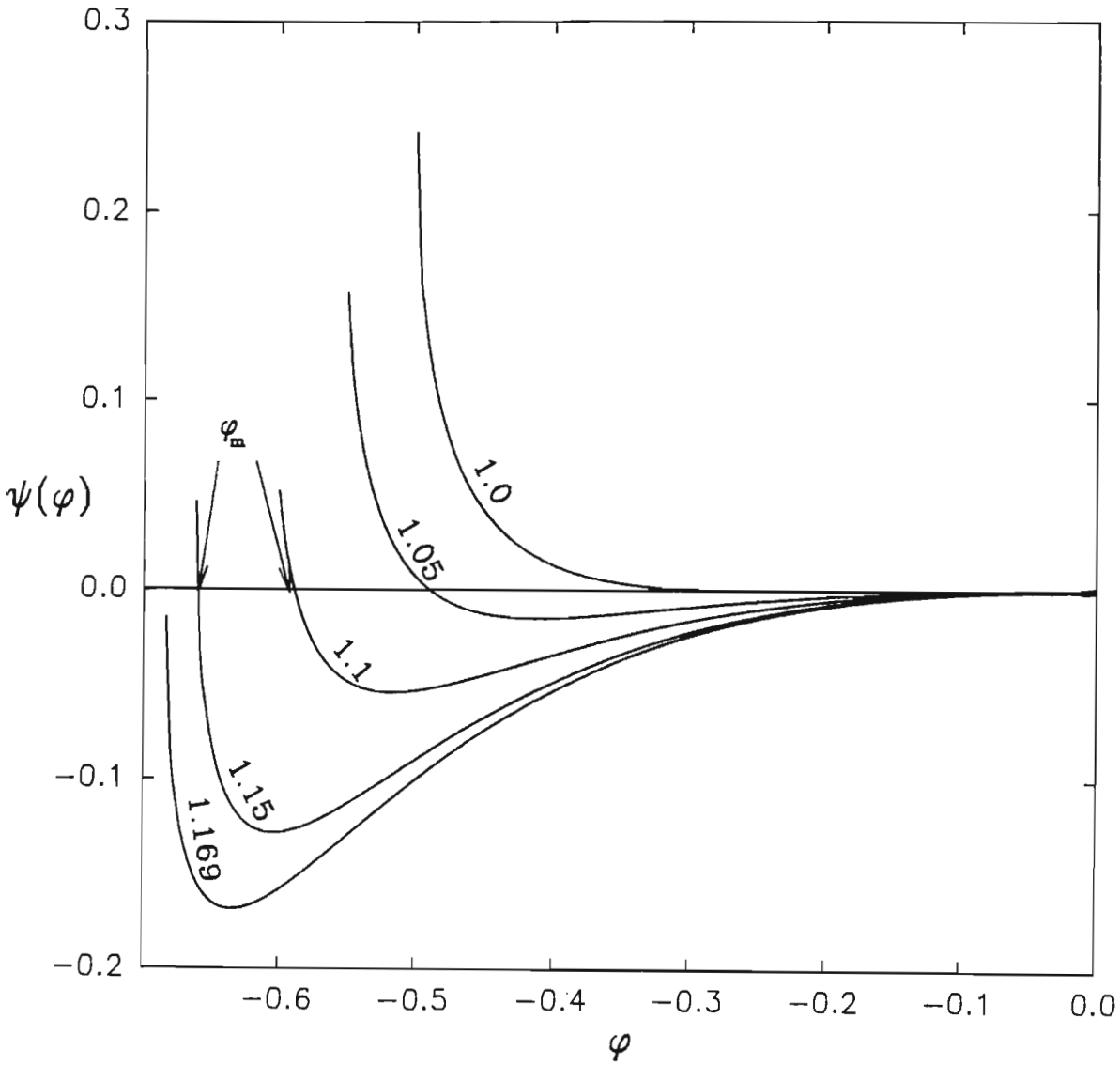

Figure 4.11: Typical forms of the large amplitude Sagdeev potential $\psi(\phi)$ for compressive solitons. The parameter labelling the curves is the Mach number M. The other fixed plasma parameters are $N_{eo} = 0$, $T_c/T_h = 0.05$ and $N_{co}/N_{ho} = 0.25$.

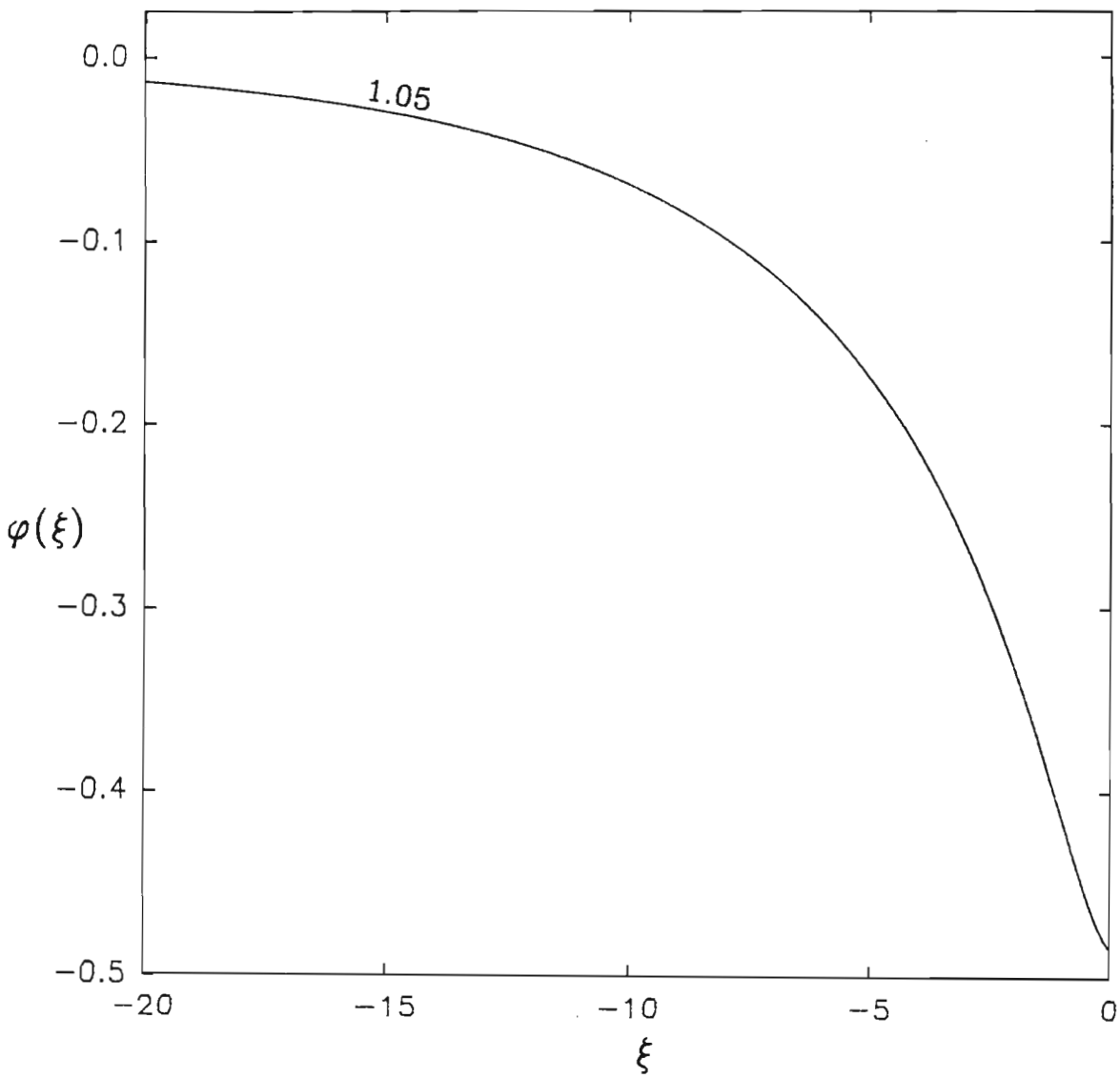

Figure 4.12: The soliton potential half-profile corresponding to the curve $M = 1.05$ in Figure 4.11.

that the normalized dust density is given by $n'_d = M/(M^2 + 2\phi)^{\frac{1}{2}}$. For $\phi < 0$(the case under study) real values of n'_d are possible for values of M satisfying $M^2 > 2 \mid \phi \mid$. The upper limit on M in Figure 4.11 is determined by this condition. The lower limit of supersonic solitons ($M > 1$) is the same as that for the rarefactive solitons. It is seen from the above expression for n'_d that when ϕ reaches its maximum negative value of ϕ_m, n'_d attains its largest positive value, corresponding to a compressive soliton structure.

The reason for selecting the value of $N_{co}/N_{ho} = 0.25$ in Figures 4.11 and 4.12 can be seen from Figure 4.13 where the soliton amplitude ϕ_m is shown as a function of the normalized cool ion density N_{co} for different values of M, with $N_{eo} = 0$ and $T_c/T_h = 0.05$. For $1 < M \leq 1.46$, the lowest possible value of N_{co} for soliton formation is found to be 0.1265, which we note is higher than the lower value (<0.1) obtained for rarefactive solitons (Figure 4.9). The lower left boundary (broken line) is due to the condition $M^2 > 2 \mid \phi \mid$.

A direct comparison with Figure 4.9 is presented by Figure 4.14 where we plot ϕ_m against N_{co}/N_{ho} for $M = 1.1, T_c/T_h = 0.05, T_e/T_h = 10$ and vary N_{eo}. We note that the lower cut-off of N_{co}/N_{ho} is higher in the latter case than in the former, while no upper limit of N_{co}/N_{ho} exists in the latter as compared to the former. Furthermore, as the value of N_{eo} increases the range of N_{co}/N_{ho} values for soliton formation increases in Figure 4.14, the opposite behaviour is seen in Figure 4.9.

For different values of M, Figure 4.15 shows the variation of the soliton amplitude ϕ_m with the cool to hot ion temperature ratio T_c/T_h. For a comparative study we have selected the same values of Mach numbers as used for rarefactive solitons in Figure 4.4. In Figure 4.15, as the value of M increases, solitons are found for a narrower

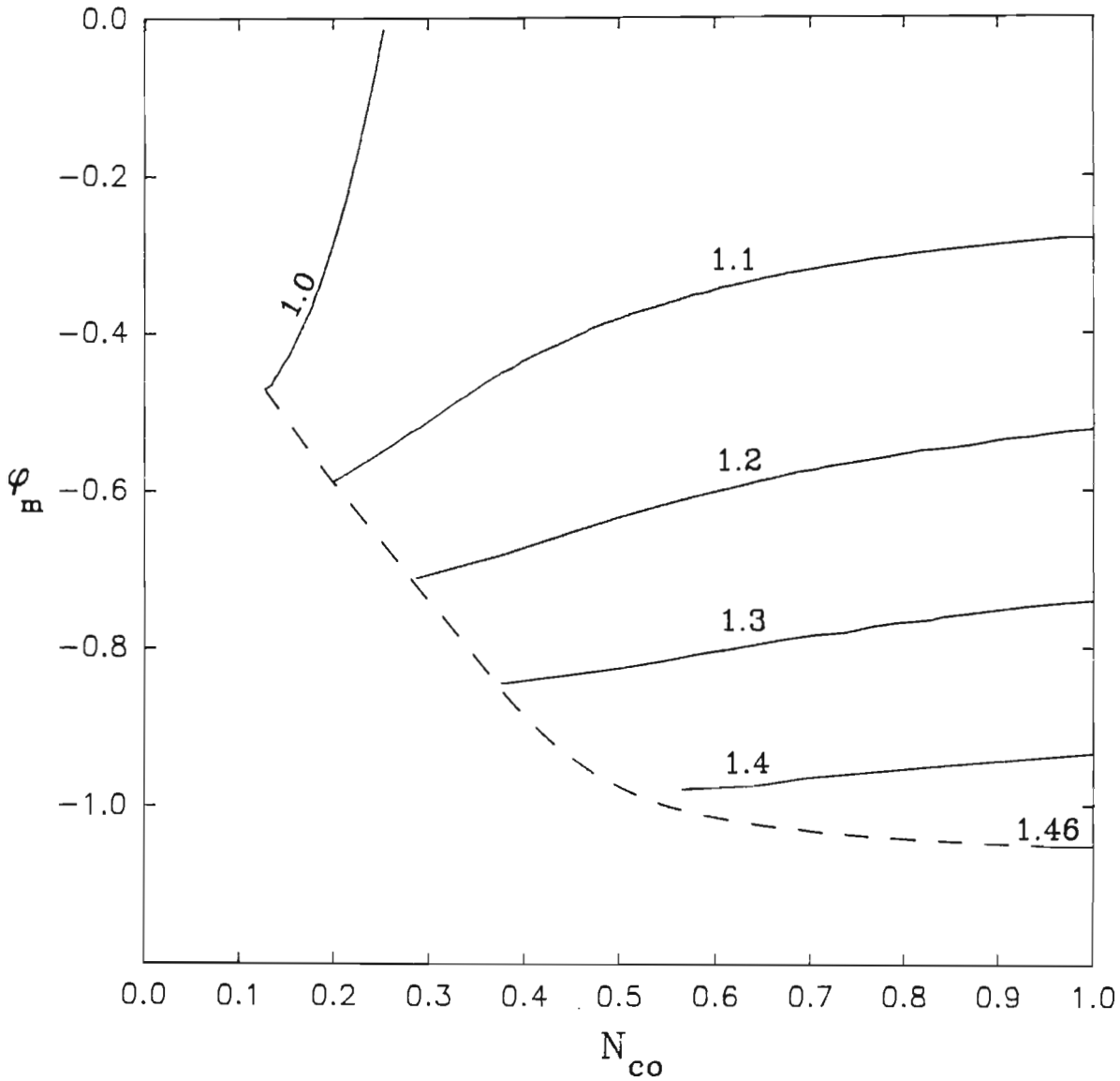

Figure 4.13: Variation of the soliton amplitude ϕ_m with the cool ion density N_{co}. The parameter labelling the curves is the Mach number M. The other fixed parameters are as in Figure 4.11.

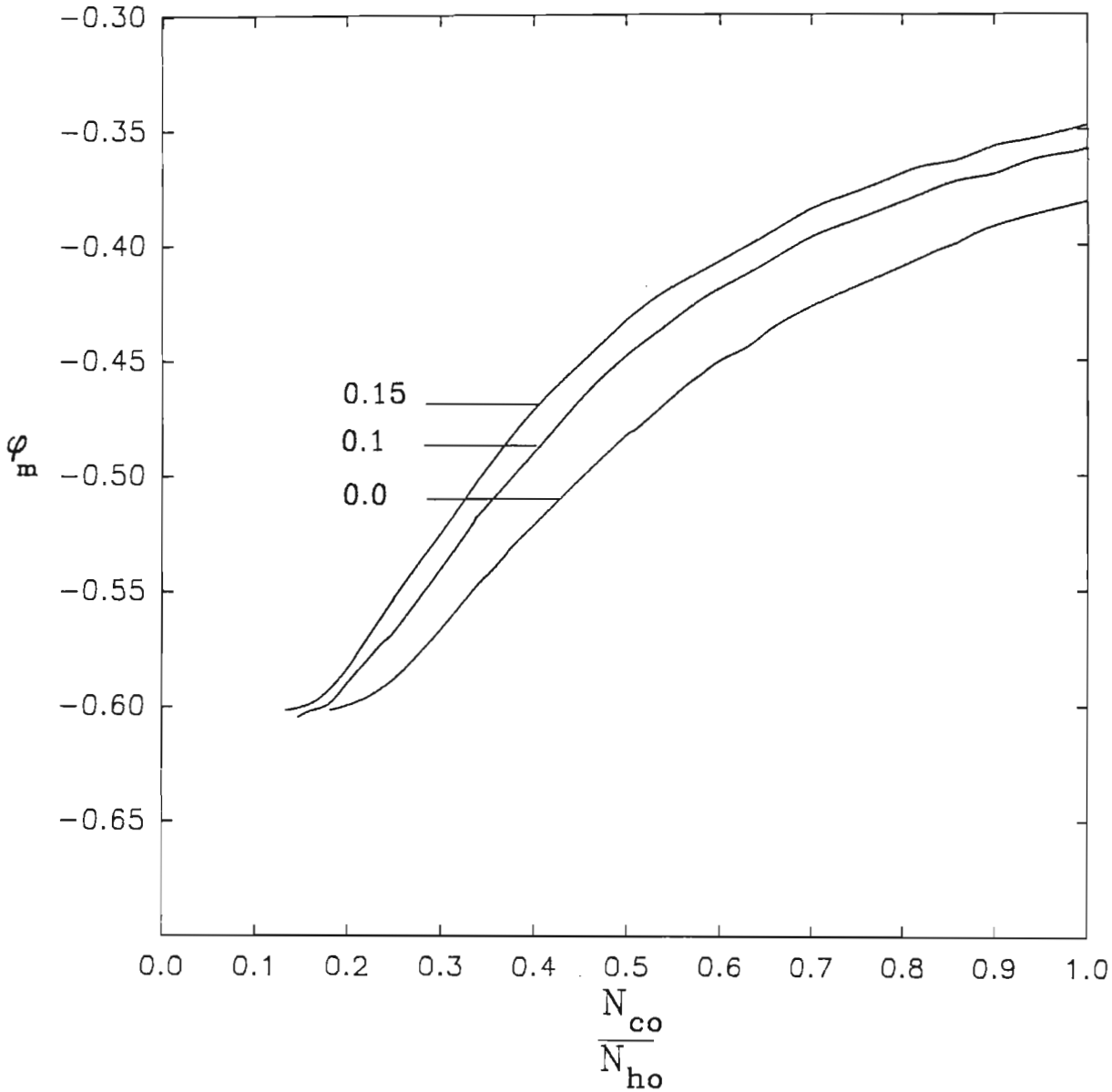

Figure 4.14: The soliton amplitude ϕ_m as a function of the cool to hot ion density ratio N_{co}/N_{ho} for $T_e/T_h = 10$. The parameter labelling the curves is N_{eo}. The other fixed parameters are $T_c/T_h = 0.05$ and $M = 1.1$.

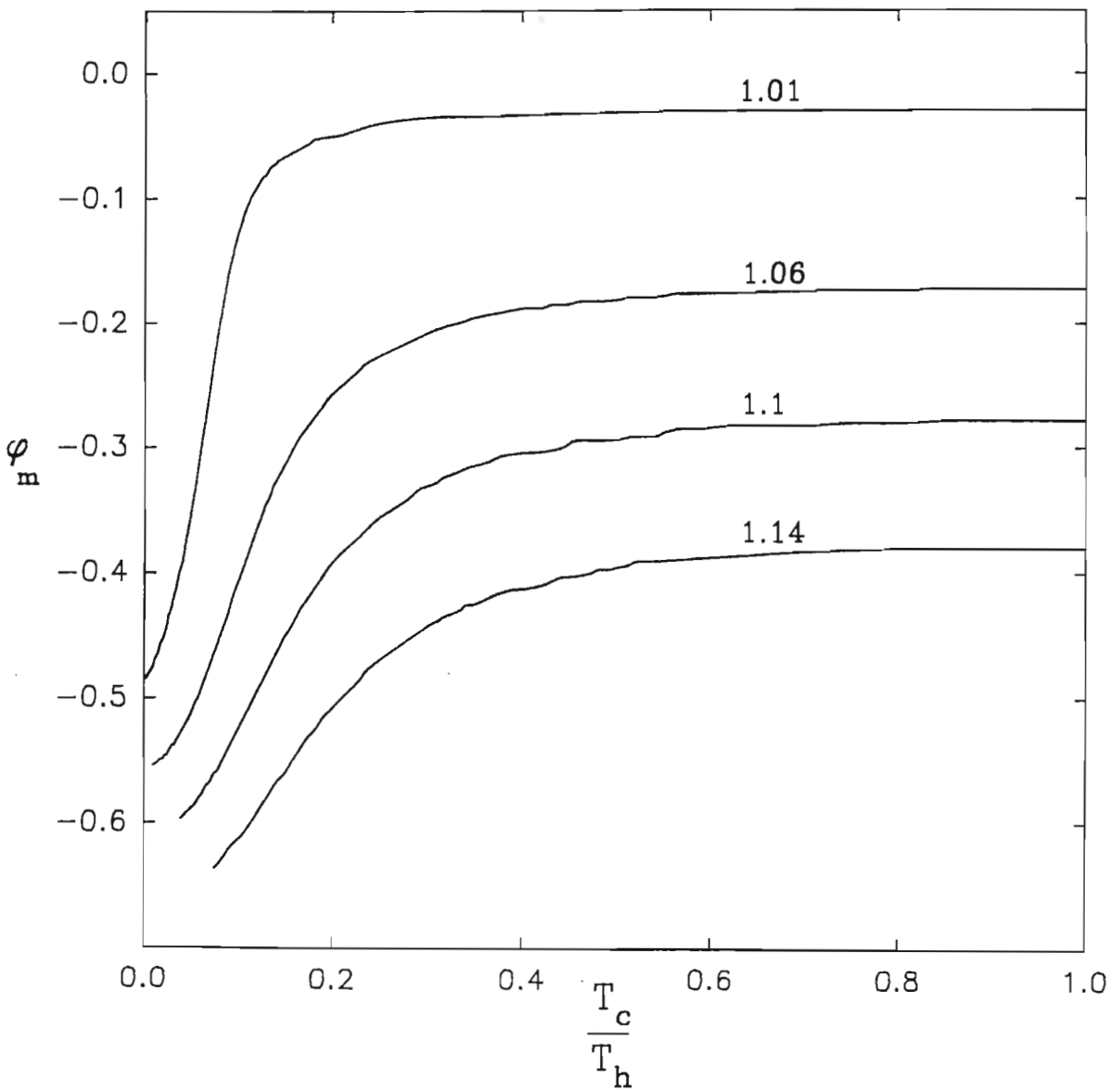

Figure 4.15: Variation of the soliton amplitude ϕ_m with the ratio of cool to hot ion temperature T_c/T_h. The parameter labelling the curves is the Mach number M. Other fixed parameters are as in Figure 4.11.

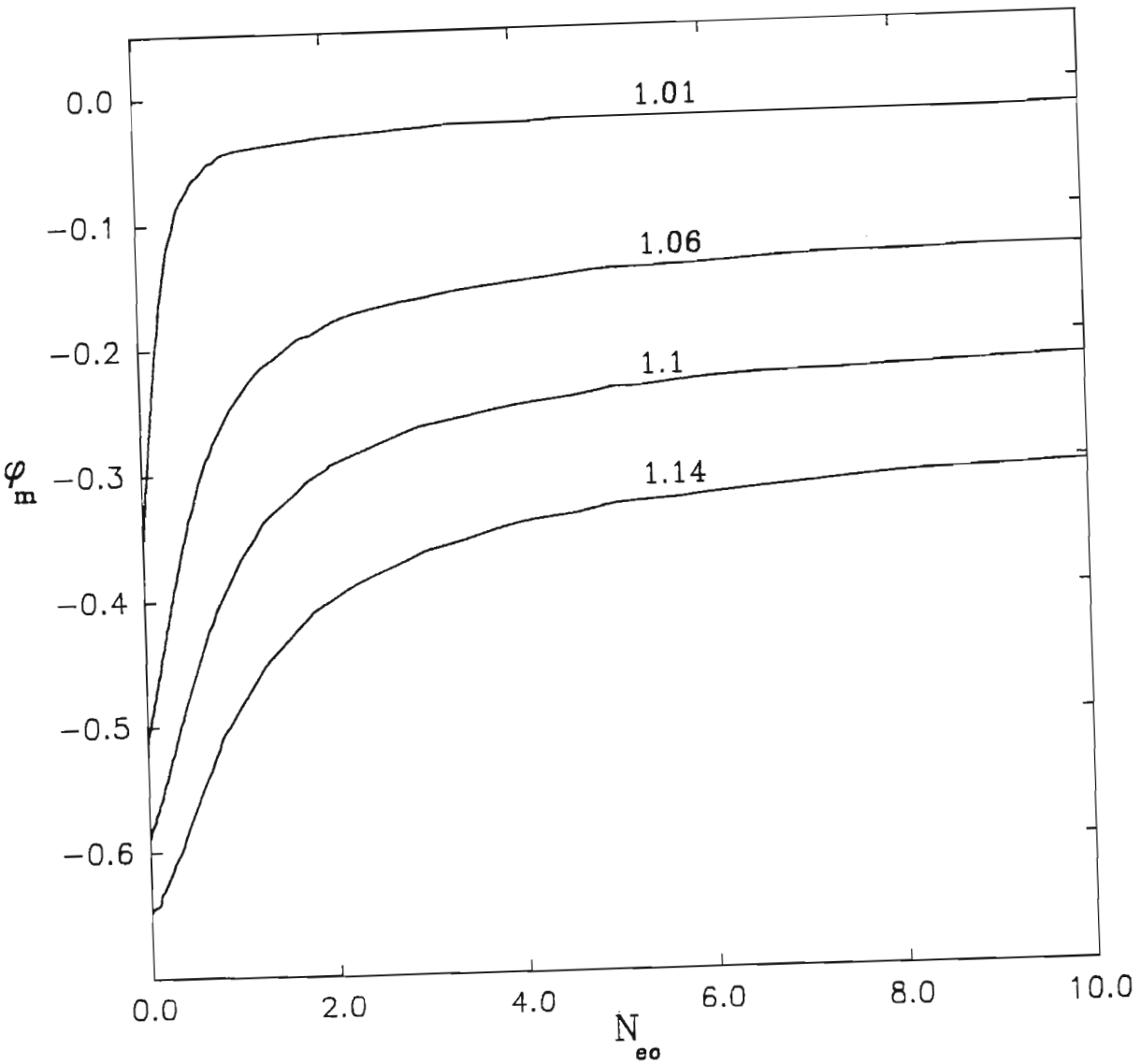

Figure 4.16: The soliton amplitude ϕ_m as a function of the normalised electron density N_{eo}. The parameter labelling the curves is the Mach number M. Here $T_e/T_h = 10$, with the other fixed parameters as in Figure 4.11.

range of T_c/T_h values, with $\mid \phi_m \mid$ decreasing with increasing T_c/T_h. Changes in ϕ_m are small for larger values of T_c/T_h. For each value of M, there exists a lower threshold of T_c/T_h below which solitons are not found. For the rarefactive studies (Figure 4.4), solitons do not exist beyond an upper threshold value of T_c/T_h, while $\mid \phi_m \mid$ increases with T_c/T_h.

Figure 4.16 shows the dependence of the soliton amplitude ϕ_m on the normalized electron density N_{eo}. The parameter labelling the curves is the the Mach number M. As we increase N_{eo}, for values satisfying $N_{eo} > 5$, the increase in ϕ_m is found to be very gradual. In contrast to Figure 4.6, in Figure 4.16 the solitons are possible over a wider range of N_{eo} values. As a function of M, it is seen from the latter that $\mid \phi_m \mid$ increases with M, as is the case in the former.

4.4 Conclusion

In this chapter we have investigated large amplitude solitons in an unmagnetised dusty plasma consisting of electrons, two species of ions (hot and cool) and a cold dust fluid consisting of negatively-charged particles. The density distributions of the electrons and the ions have been taken to be of the Boltzmann type, while the dynamics of the dust fluid is governed by the fluid equations. The study is carried out for both the rarefactive (amplitude $\phi_m > 0$) and compressive (amplitude $\phi_m < 0$) solitons.

For rarefactive solitons, in the absence of the electron component, a study of the dependence of soliton amplitude (ϕ_m) on the cool to hot ion temperature ratio T_c/T_h for different values of M, as well as on the Mach numbers for different T_c/T_h ratios, show that the range in which the solitons are found narrows sharply as M increases

in the former case and as T_c/T_h increases slightly in the latter case. Only supersonic ($M > 1$) solitons are found to exist. Typically for $T_c/T_h = 0.05$, solitons do not exist for M >1.159. At the threshold a double layer potential structure is formed. Our results also show that low Mach number solitons are possible over a wide range of T_c/T_h values.

When we consider the effect of a finite electron population it is found that for each value of Mach number, the soliton amplitude increases with increasing electron density (N_{eo}) but with an upper limit of N_{eo} beyond which solitons are not found. Low Mach number solitons exist over a wide range of N_{eo} values. On the otherhand, for a fixed N_{eo}, ϕ_m decreases with increasing T_e/T_h, and decreasing N_{co}/N_{ho}, for a fixed value of M. In both instances there are lower cut offs (of T_e/T_h and N_{co}/N_{ho} respectively) below which no solitons are found to exist.

For the compressive solitons, as for the rarefactive solitons, we find that the Mach number M should not become subsonic for soliton formation to be possible. On the otherhand, there is also an upper value of M beyond which solitons do not occur. This value is determined by the condition that the dust density becomes complex.

A variation of the ratio of cool to hot ion density N_{co}/N_{ho} shows that the compressive solitons have a larger lower cut-off for soliton formation than the rarefactive solitons, with the range of N_{co}/N_{ho} values (for solitons to occur) increasing (decreasing) with the electron density N_{eo} for the former (latter).

As the cool to hot ion temperature ratio T_c/T_h is varied for a given M-value, the compressive solutions have a lower threshold value below which solitons do not occur, with the amplitude $\mid \phi_m \mid$ decreasing with T_c/T_h. The opposite behaviour is found for the rarefactive solitons. A study of the dependence of ϕ_m on the electron density N_{eo}

shows that for a given Mach number, the range of N_{eo} values for solitons to occur is much larger in the case of the compressive solitons than for the rarefactive solitons. The upper cut-off value of N_{eo} observed for the rarefactive solitons is not seen for their compressive counterparts.

Part of the results of this chapter have already been published in the journal Planetary and Space Science (S. Vidhya Lakshmi and R. Bharuthram 1994).

Chapter 5

A KINETIC THEORY APPROACH TO SMALL AMPLITUDE SOLITONS IN A DUSTY PLASMA

5.1 Introduction

In the previous chapter we investigated arbitrary amplitude solitons in a dusty plasma via the fluid equations. Here, using the same plasma model as in chapter four, a study is made via the reductive perturbation technique of small amplitude or weak solitons in a dusty plasma. The initial study is in terms of kinetic theory, using a Vlasov-Poisson system. The associated Korteweg de Vries (KdV) equation is derived. Then the analogous problem is solved via the fluid equations. Differences between the coefficients of the two KdV equations are discussed, as well as those between the

corresponding stationary soliton profiles.

Using the fluid equations Washimi and Taniuti (1966) showed how weak solitary waves propagate in a plasma of cold ions and isothermal electrons by deriving a nonlinear partial differential equation in the form of a Korteweg de Vries equation. Later this has been extensively studied, both theoretically and experimentally by a number of authors (Taniuti and Wei, 1968; Ikezi et al. 1970; Ikezi 1973; Nakamura 1982). The kinetic treatment here for a dusty plasma is based on the work done by Kato et al. (1972) who obtained a kinetic KdV equation for ion-acoustic solitons by considering a Vlasov-Poisson system.

5.2 Derivation of the kinetic KdV equation

We start by considering a collisionless and unmagnetised dusty plasma. We assume that the massive dust particles are described by the Vlasov equation and the particle densities of the massless electrons and ions given by the Boltzmann distribution:

$$\frac{\partial f_d}{\partial t} + v\frac{\partial f_d}{\partial x} + \frac{Z_d e}{m}\frac{\partial \phi}{\partial x}\frac{\partial f_d}{\partial v} = 0\,, \tag{5.1}$$

$$n_e = n_{eo}\exp\left(\frac{e\phi}{T_e}\right), \tag{5.2}$$

$$n_i = n_{io}\exp\left(\frac{-e\phi}{T_i}\right), \tag{5.3}$$

where f_d is the dust velocity distribution function and ϕ is the electrostatic potential. $Z_d e$ and m are the charge and mass of the dust particle, n_{eo} (n_{io}) is the equilibrium number density of the electrons (ions), T_e (T_i) is the temperature of the electrons (ions). The above equations couple with each other through the Poisson equation:

$$\frac{\partial^2 \phi}{\partial x^2} = 4\pi e(n_e + Z_d n_d - n_i)\,. \tag{5.4}$$

Quasineutrality at equilibrium requires

$$n_{eo} + Z_d n_{do} = n_{io}\,. \tag{5.5}$$

To solve equation (5.1) we consider the following characteristic equations over which f_d is constant.

$$\frac{dx}{dt} = u\,, \tag{5.6}$$

$$\frac{du}{dt} = Z_d \frac{\partial \phi}{\partial x}\,, \tag{5.7}$$

$$Z_d \frac{\partial^2 \phi}{\partial x^2} = (n_e + n_d - n_i)\,, \tag{5.8}$$

$$\left.\begin{aligned} n_e &= n_{eo} e^{\phi} \\ n_i &= n_{io} e^{-\sigma\phi} \end{aligned}\right\} \tag{5.9}$$

where $\sigma(= T_e/T_i)$ is the ratio of the electron temperature to the ion temperature. In equations (5.6) - (5.9) we have normalised densities by $Z_d n_{do}$, the potential by T_e/e , the characteristic velocity by the dust-acoustic speed $c_{sd} = (T_e/m)^{\frac{1}{2}}$, the characteristic length by $\lambda_d = \left(\frac{T_e}{4\pi n_{do} Z_d^2 e^2}\right)^{\frac{1}{2}}$, and the time is in units of the inverse plasma period $\omega_p^{-1} = \left(\frac{4\pi n_{do} Z_d^2 e^2}{m}\right)^{-\frac{1}{2}}$.

In order to derive the KdV equation, the order of perturbation may be deduced from the fluid model, which gives the scaling

$$\xi = \epsilon^{\frac{1}{2}}(x - \lambda t)\,, \qquad \tau = \epsilon^{\frac{3}{2}} t\,, \tag{5.10}$$

where λ is the unknown phase velocity to be obtained later and ϵ is the expansion parameter. The plasma parameters are now expanded asymptotically as a power series in ϵ as

$$u = u_o + \epsilon u_1 + \epsilon^2 u_2 + \ldots\,, \tag{5.11}$$

$$\phi = \epsilon\phi_1 + \epsilon^2\phi_2 + \ldots, \tag{5.12}$$

$$x - (x_o + u_o t) = \epsilon^{\frac{1}{2}} x_1 + \epsilon^{\frac{3}{2}} x_2 + \ldots, \tag{5.13}$$

in which x_o and u_o are the initial position and velocity, respectively. From (5.10) we obtain the following transformations

$$\begin{aligned} \frac{d}{dt} &= \epsilon^{\frac{1}{2}}(u-\lambda)\frac{\partial}{\partial\xi} + \epsilon^{\frac{3}{2}}\frac{\partial}{\partial\tau} \\ \frac{d}{dx} &= \epsilon^{\frac{1}{2}}\frac{\partial}{\partial\xi}. \end{aligned}$$

Using equations (5.10) - (5.13), equations (5.6) and (5.7) can be written as

$$\epsilon\,(u_o - \lambda + \epsilon u_1 + \epsilon^2 u_2)\frac{\partial}{\partial\xi}(x_1 + \epsilon x_2) + \epsilon^2\frac{\partial}{\partial\tau}(x_1 + \epsilon x_2) = \epsilon u_1 + \epsilon^2 u_2\,, \tag{5.14}$$

$$\begin{aligned} \epsilon^{\frac{1}{2}}\,(u_o - \lambda + \epsilon u_1 + \epsilon^2 u_2)\frac{\partial}{\partial\xi}(\epsilon u_1 + \epsilon^2 u_2) + \epsilon^{\frac{3}{2}}\frac{\partial}{\partial\tau}(\epsilon u_1 + \epsilon^2 u_2) \\ = Z_d\,\epsilon^{\frac{1}{2}}\frac{\partial}{\partial\xi}(\epsilon\phi_1 + \epsilon^2\phi_2). \end{aligned} \tag{5.15}$$

Collecting the lowest order terms in ϵ in the above equations (5.14) and (5.15), we have

$$\begin{aligned} (u_o - \lambda)\frac{\partial x_1}{\partial\xi} &= u_1\,, \\ (u_o - \lambda)\frac{\partial u_1}{\partial\xi} &= Z_d\frac{\partial\phi_1}{\partial\xi}. \end{aligned}$$

Similarly, to the next higher order in ϵ gives the following relations

$$\begin{aligned} (u_o - \lambda)\frac{\partial x_2}{\partial\xi} + u_1\frac{\partial x_1}{\partial\xi} + \frac{\partial x_1}{\partial\tau} &= u_2 \\ (u_o - \lambda)\frac{\partial u_2}{\partial\xi} + u_1\frac{\partial u_1}{\partial\xi} + \frac{\partial u_1}{\partial\tau} - Z_d\frac{\partial\phi_2}{\partial\xi} &= 0 \end{aligned}$$

which are easily integrated to give

$$x_1 = \frac{Z_d}{(u_o - \lambda)^2}\int_{-\infty}^{\xi}\phi_1 d\xi \tag{5.16}$$

$$u_1 = \frac{Z_d}{(u_o - \lambda)}\phi_1 \tag{5.17}$$

$$u_2 = -\frac{Z_d}{(u_o - \lambda)^2}\int_{-\infty}^{\xi}\frac{\partial\phi_1}{\partial\tau}d\xi + \frac{Z_d}{(u_o - \lambda)}\phi_2 - \frac{Z_d^2}{2(u_o - \lambda)^3}\phi_1^2 \tag{5.18}$$

We calculate the dust density $n_d(\xi,\tau) = \int f_d(u,\xi,\tau)du$ from the equation which is valid along the particle trajectory:

$$\begin{aligned} f_d(u,\xi,\tau) &= f_d(u_o, \epsilon^{\frac{1}{2}}x_o, o) = f_o(u_o) \\ &= f_o(u - \epsilon u_1 - \epsilon^2 u_2) \\ &= f_o(u) - \epsilon u_1\frac{\partial f_o}{\partial u} + \epsilon^2\left(-u_2\frac{\partial f_o}{\partial u} + \frac{1}{2}u_1^2\frac{\partial^2 f_o}{\partial u^2}\right). \end{aligned} \tag{5.19}$$

From equation (5.9) we have

$$\left.\begin{aligned} n_e &= n_{eo}\left(1 + \epsilon\phi_1 + \epsilon^2\phi_2 + \tfrac{1}{2}\epsilon^2\phi_1^2\right) \\ n_i &= n_{io}\left(1 - \sigma\epsilon\phi_1 - \sigma\epsilon^2\phi_2 + \tfrac{1}{2}\sigma^2\epsilon^2\phi_1^2\right). \end{aligned}\right\} \tag{5.20}$$

Using equations (5.17) and (5.18), (5.19) can be written as

$$\begin{aligned} f_d = f_o(u) &- \frac{Z_d}{(u_o - \lambda)}\epsilon\phi_1\frac{\partial f_o}{\partial u} + \epsilon^2\left[\frac{Z_d}{(u_o - \lambda)^2}\frac{\partial f_o}{\partial u}\int_{-\infty}^{\xi}\frac{\partial\phi_1}{\partial\tau}d\xi\right. \\ &\left. - \frac{Z_d}{(u_o - \lambda)}\phi_2\frac{\partial f_o}{\partial u} + \frac{Z_d^2}{2(u_o - \lambda)^3}\phi_1^2\frac{\partial f_o}{\partial u} + \frac{Z_d^2}{2(u_o - \lambda)^2}\phi_1^2\frac{\partial^2 f_o}{\partial u^2}\right]. \end{aligned} \tag{5.21}$$

Substituting (5.20) and n_d (calculated via (5.21)) into the Poisson equation (5.8), using equation (5.11) to express u_o in terms of $u, u_1, ...$, we have

$$\begin{aligned} Z_d\,\epsilon\left[\epsilon\frac{\partial^2\phi_1}{\partial\xi^2} + ...\right] &= n_{eo}\left[1 + \epsilon\phi_1 + \epsilon^2\phi_2 + \frac{1}{2}\epsilon^2\phi_1^2\right] \\ &\quad - n_{io}\left[1 - \sigma\left(\epsilon\phi_1 + \epsilon^2\phi_2\right) + \frac{\sigma^2}{2}\epsilon^2\phi_1^2\right] \\ &\quad + \int_{-\infty}^{+\infty} f_o(u)du - Z_d\,\epsilon\int_{-\infty}^{+\infty}\frac{\partial f_o}{\partial u}\frac{\phi_1}{u - \lambda}du \end{aligned}$$

$$+\epsilon^2 \int_{-\infty}^{+\infty} \left[\frac{Z_d}{(u-\lambda)^2} \frac{\partial f_o}{\partial u} \int_{-\infty}^{\xi} \frac{\partial \phi_1}{\partial \tau} d\xi \right.$$
$$- \frac{Z_d}{(u-\lambda)} \phi_2 \frac{\partial f_o}{\partial u} + \frac{Z_d^2}{2(u-\lambda)^3} \phi_1^2 \frac{\partial f_o}{\partial u}$$
$$\left. + \frac{Z_d^2}{2(u-\lambda)^2} \phi_1^2 \frac{\partial^2 f_o}{\partial u^2} - \frac{Z_d^2}{(u-\lambda)^3} \phi_1^2 \frac{\partial f_o}{\partial u} \right] du. \qquad (5.22)$$

To zero order, $n_{eo} - n_{io} = \int f_o(u)du(=1) = n_{do}$ in normalized form.

Collecting the lowest order term in $\epsilon(\epsilon^1)$ in the above equation, we obtain

$$n_{eo} + \sigma n_{io} = Z_d \int_{-\infty}^{+\infty} \frac{\partial f_o}{\partial u} \frac{du}{u-\lambda} \qquad (5.23)$$

from which the phase velocity λ of the wave is obtained for a given velocity distribution f_o. For a Maxwellian distribution,

$$f_o = (2\pi\sigma_1)^{-\frac{1}{2}} exp\left(-\frac{u^2}{2\sigma_1}\right),$$

we find

$$\lambda = \pm(Z + 3\sigma_1)^{\frac{1}{2}} \qquad (5.24)$$

where $Z = \frac{Z_d}{n_{eo}+\sigma n_{io}}$ and $\sigma_1(= T_d/T_e)$ is the ratio of the temperature of the dust particle to that of the electron.

The next higher order term in $\epsilon(\epsilon^2)$ gives

$$Z_d \frac{\partial^2 \phi}{\partial \xi^2} = \frac{n_{eo}}{2}\phi_1^2 - \frac{\sigma^2 n_{io}}{2}\phi_1^2 + \int_{-\infty}^{+\infty} \frac{Z_d}{(u-\lambda)^2} \frac{\partial f_o}{\partial u} \int_{-\infty}^{\xi} \frac{\partial \phi_1}{\partial \tau} d\xi du$$
$$+ \int_{-\infty}^{+\infty} \frac{Z_d^2}{2(u-\lambda)^3} \phi_1^2 \frac{\partial f_o}{\partial u} du + \int_{-\infty}^{+\infty} \frac{Z_d^2}{2(u-\lambda)^2} \phi_1^2 \frac{\partial^2 f_o}{\partial u^2}$$
$$- \int_{-\infty}^{+\infty} \frac{Z_d^2}{(u-\lambda)^3} \phi_1^2 \frac{\partial f_o}{\partial u} du,$$

which after differentiating both sides of the equation w.r.t ξ gives

$$0 = Z_d \frac{\partial^3 \phi_1}{\partial \xi^3} - Z_d \frac{\partial \phi_1}{\partial \tau} \int_{-\infty}^{+\infty} (u-\lambda)^{-2} \frac{\partial f_o}{\partial u} du$$

$$+\phi_1 \frac{\partial \phi_1}{\partial \xi}\left[-n_{eo}+\sigma^2 n_{io}+Z_d^2\int_{-\infty}^{+\infty}(u-\lambda)^{-3}\frac{\partial f_o}{\partial u}du\right.$$
$$\left.-Z_d^2\int_{-\infty}^{+\infty}(u-\lambda)^{-2}\frac{\partial^2 f_o}{\partial u^2}du\right],$$

which can be written in the form of a KdV equation as

$$\gamma_k \frac{\partial \phi_1}{\partial \tau}+\alpha_k\,\phi_1\frac{\partial \phi_1}{\partial \xi}+\frac{\partial^3 \phi_1}{\partial \xi^3}=0\,, \tag{5.25}$$

where

$$\alpha_k = \frac{1}{Z_d}\left[\sigma^2 n_{io}-n_{eo}-Z_d^2\int_{-\infty}^{+\infty}(u-\lambda)^{-3}\frac{\partial f_o}{\partial u}du\right], \tag{5.26}$$

$$\gamma_k = -\int_{-\infty}^{+\infty}(u-\lambda)^{-2}\frac{\partial f_o}{\partial u}du\,. \tag{5.27}$$

Hence equation (5.25) is the general KdV for dust-acoustic waves obtained via kinetic theory. It is seen from (5.26) and (5.27) the coefficients α_k and γ_k are obtained, once the equilibrium velocity distribution $f_o(u)$ of the dust particles are given.

5.3 Derivation of the fluid KdV equation

We compare the kinetic KdV equation (5.25) with that derived from pure fluid theory. The basic set of fluid equations in the dimensionless form are

the dust continuity equation:

$$\frac{\partial n_d}{\partial t}+\frac{\partial}{\partial x}(n_d u)=0\,, \tag{5.28}$$

the dust momentum equation:

$$\frac{\partial u}{\partial t}+u\frac{\partial u}{\partial x}=Z_d\frac{\partial \phi}{\partial x}\,, \tag{5.29}$$

and the Poisson equation

$$Z_d\frac{\partial^2 \phi}{\partial x^2}=n_e+n_d-n_i\,, \tag{5.30}$$

where the dimensionless parameters are defined as in kinetic theory.

We introduce the stretched space-time variables as given in (5.10) and use the power series expansion (5.11) and (5.12) for the quantities u and ϕ. Then expanding n_d, we have

$$\left.\begin{aligned} n_d &= 1 + \epsilon n_{d1} + \epsilon^2 n_{d2} + ... \\ u &= u_o + \epsilon u_1 + \epsilon^2 u_2 + ... \\ \phi &= \epsilon\phi_1 + \epsilon^2\phi_2 + ... \end{aligned}\right\} \tag{5.31}$$

Substituting (5.10) and (5.31) firstly in the Poisson equation (5.30) and then collecting the lowest order term in $\epsilon(\epsilon^1)$ gives

$$n_{d1} = -(n_{eo} + \sigma n_{io})\phi_1\,, \tag{5.32}$$

and the next higher order term in $\epsilon(\epsilon^2)$ yield

$$Z_d\frac{\partial^2\phi_1}{\partial\xi^2} - n_{eo}\phi_2 - \frac{n_{eo}}{2}\phi_1^2 - \sigma n_{io}\phi_2 + \frac{\sigma^2 n_{io}}{2}\phi_1^2 = n_{d2}\,. \tag{5.33}$$

Substituting (5.10) and (5.31) in (5.28) and (5.29) and then collecting the lowest order term in $\epsilon(\epsilon^{\frac{3}{2}})$ gives

$$(u_o - \lambda)\frac{\partial}{\partial\xi}n_{d1} = -\frac{\partial}{\partial\xi}u_1\,, \tag{5.34}$$

$$(u_o - \lambda)\frac{\partial}{\partial\xi}u_1 = Z_d\frac{\partial}{\partial\xi}\phi_1. \tag{5.35}$$

To the next higher order in $\epsilon(\epsilon^{\frac{5}{2}})$ we obtain

$$\frac{\partial}{\partial\tau}n_{d1} + (u_o - \lambda)\frac{\partial}{\partial\xi}n_{d2} + \frac{\partial}{\partial\xi}n_{d1}u_1 + \frac{\partial}{\partial\xi}u_2 = 0\,, \tag{5.36}$$

$$(u_o - \lambda)\frac{\partial}{\partial\xi}u_2 = -\frac{\partial u_1}{\partial\tau} - u_1\frac{\partial u_1}{\partial\xi} + Z_d\frac{\partial\phi_2}{\partial\xi}\,. \tag{5.37}$$

In equations (5.33), (5.36) and (5.37) we substitute for n_{d1} and u_1 in terms of ϕ_1 using equations (5.32), (5.34) and (5.35). Solving for n_{d2} and u_2 from (5.33) and (5.37), respectively and substituting in (5.36), we finally get the following KdV equation

$$\gamma_f \frac{\partial \phi}{\partial \tau} + \alpha_f \phi_1 \frac{\partial \phi_1}{\partial \xi} + \frac{\partial^3 \phi_1}{\partial \xi^3} = 0\,, \tag{5.38}$$

where

$$\alpha_f = \frac{1}{Z_d}\left[\sigma^2 n_{io} - n_{eo} - 3Z_d^2(u_o - \lambda)^{-4}\right]\,, \tag{5.39}$$

$$\gamma_f = -2(u_o - \lambda)^{-3}. \tag{5.40}$$

5.4 Comparison between the kinetic and the fluid KdV equations

In order to obtain the corresponding fluid equation from the kinetic KdV equation, the coefficients α_k and γ_k are evaluated for a δ - function velocity distribution, viz.

$$f_o = \delta(u - u_o)\,.$$

(Recall in normalized form, $\int f_o du = 1$)

Then

$$\alpha_k = \frac{1}{Z_d}\left[\sigma^2 n_{io} - n_{eo} - 3Z_d^2(u_o - \lambda)^{-4}\right]\,, \tag{5.41}$$

is obtained using

$$\int_{-\infty}^{+\infty} (u - \lambda)^{-3} \frac{\partial}{\partial u}\delta(u - u_o)du = \frac{3}{(u_o - \lambda)^4}\,,$$

and similarly

$$\gamma_k = -2(u_o - \lambda)^{-3}\,, \tag{5.42}$$

is obtained using

$$\int_{-\infty}^{+\infty}(u-\lambda)^{-2}\frac{\partial}{\partial u}\delta(u-u_o)du = \frac{2}{(u_o-\lambda)^3}\,.$$

It is seen that (5.41) and (5.42) are identical to (5.39) and (5.40). Thus the kinetic KdV equation is consistent in behavior. Moreover, it has the advantage of being applicable to any given velocity distribution function f_o. This will be illustrated in the next section.

5.5 Solution of the KdV equation

The KdV equation (5.38) is solved for a stationary solution in the frame defined by $\eta = \xi - M\tau$. We obtain

$$-\gamma M\frac{d\phi_1}{d\eta} + \alpha\phi_1\frac{d\phi_1}{d\eta} + \frac{d^3\phi_1}{d\eta^3} \tag{5.43}$$

where we drop the subscripts on γ and α. We find the solution of this equation by integrating with the boundary conditions

$$\phi_1(\eta)\,,\frac{d\phi_1}{d\eta}\,,\frac{d^2\phi_1}{d\eta^2} \to 0 \quad \text{for} \quad \pm\eta \to \infty. \tag{5.44}$$

One then obtains

$$\frac{1}{2}\left[\frac{d\phi_1}{d\eta}\right]^2 + \psi(\phi_1) = 0\,, \tag{5.45}$$

where

$$\psi(\phi_1) = \frac{-\gamma M}{2}\phi_1^2 + \frac{\alpha}{6}\phi_1^3\,.$$

Integration (5.45) results in the soliton solution

$$\phi_1 = \phi_o\, sech^2(\delta\eta) \tag{5.46}$$

where $\phi_o = \frac{3\gamma M}{\alpha}$ is the amplitude and $\delta = \frac{(\gamma M)^{\frac{1}{2}}}{2}$ is the width of the dust-acoustic solitary wave.

The soliton profile corresponding to (5.46) is shown in Figure (5.1). In Figure (5.2) is displayed the soliton profile obtained from the kinetic KdV equation (5.25) for a Maxwellian velocity distribution (see expression for f_o preceeding equation (5.24)). The chosen parameters for these curves were $n_{eo} = 1.0, n_{io} = 2.0, \sigma(= T_e/T_i) = 10.0, \sigma_1(= T_d/T_e) = 0.01, M = 1.0, Z_d = 100$ and $u_o = 10.0$. We note that a comparison of the two curves is not exact, since no thermal effects are considered in the fluid model, while in the kinetic approach no equilibrium drift is allowed for.

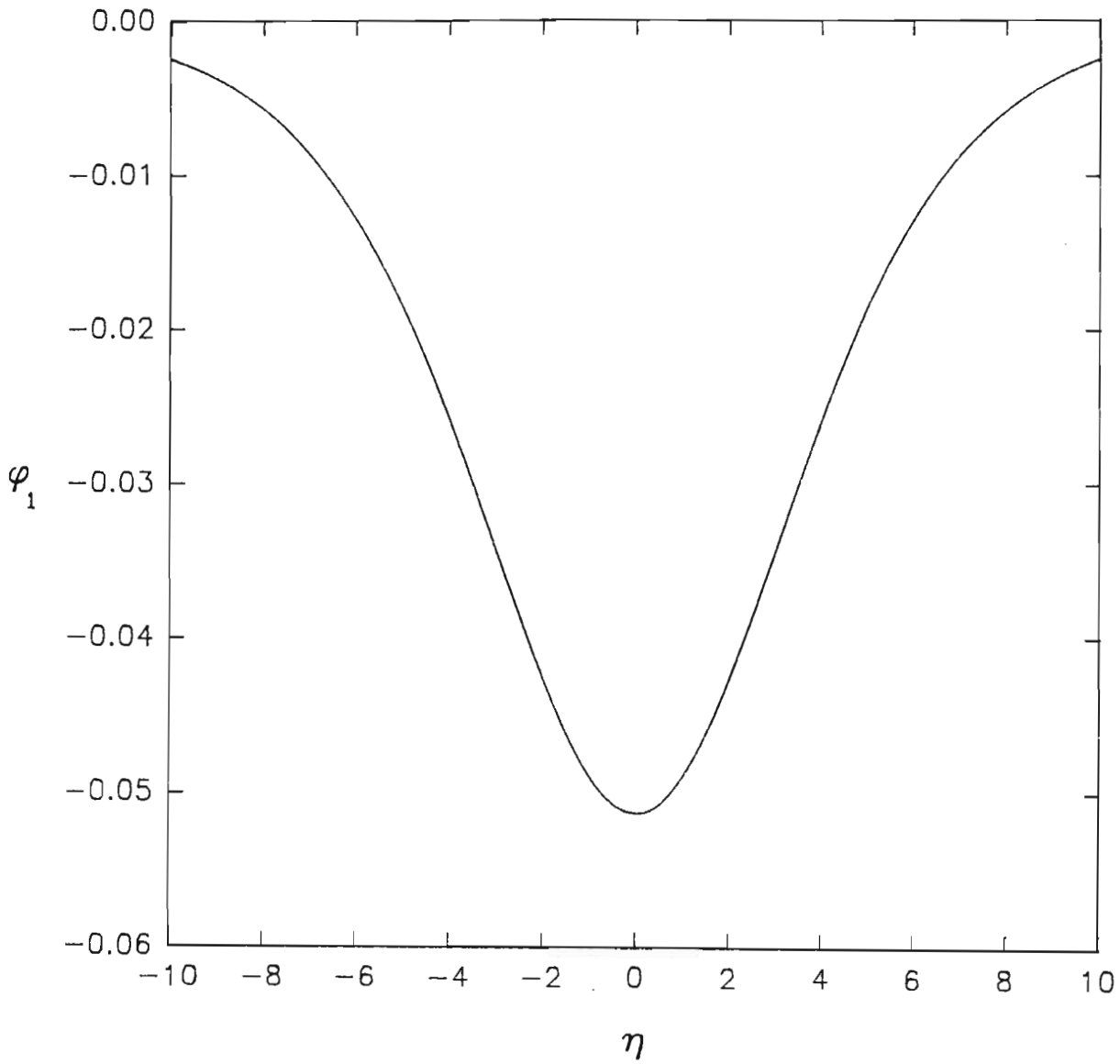

Figure 5.1: The soliton profile satisfying the fluid theory.

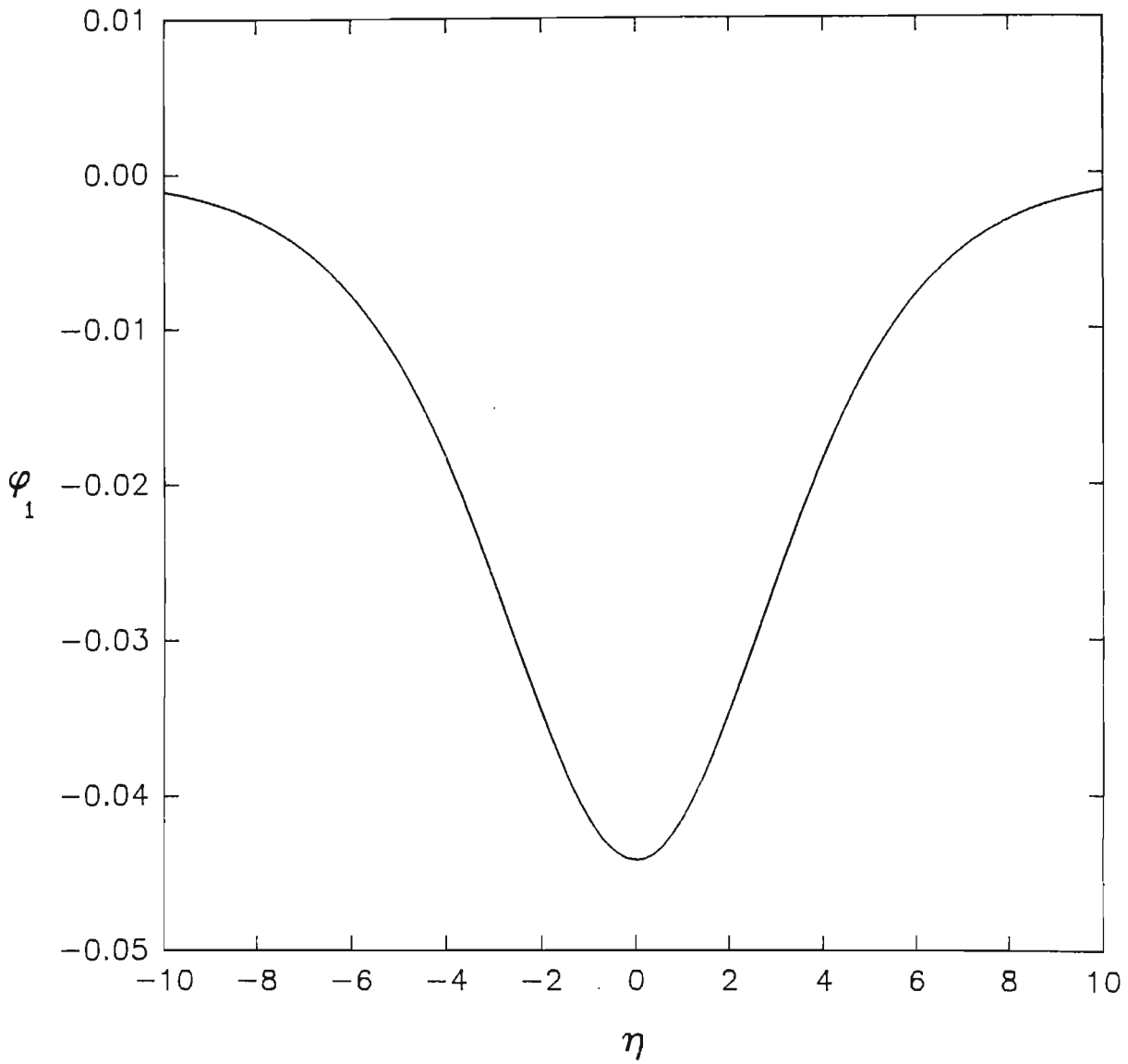

Figure 5.2: The soliton profile satisfying the kinetic theory.

Chapter 6

CONCLUSIONS

Recently, there has been much interest in the properties and behaviour of dusty plasmas as they have been increasingly observed in asteriod zones, planetary rings and magnetospheres (in those of Jupiter, Saturn and Uranus by the voyager space craft), cometary environment (in the vicinity of comet Giacobini - Zinner by the ICE satellite), as well as the lower part of the Earth's ionosphere (Whipple et al., 1985; Gendrin, 1991). Moreover, such plasmas are being increasingly studied in laboratory experiments (Sheehan et al., 1990; Carlisle et al., 1991; Bouchoule et al., 1991). In this thesis, some aspects of electrostatic wave phenomena in dusty plasmas have been investigated.

In chapter 2, the effect of Debye shielding in a dusty plasma was examined by treating electrons and ions as point particles with Boltzmann density distributions, while the massive, negatively charged dust particles were stationary. For weak electrostatic potentials, the effective Debye length (λ'_D) was found to be smaller than that in a pure electron - ion plasma. For small values of T_e/T_i, λ'_D decreases with electron density and when $T_e/T_i \gg 1$, the electrons were found to play little or no role in Debye

shielding. When an approximate analytical solution of the Poisson equation (using spherical coordinates) was compared with a numerical solution (using a backward differencing scheme) of the complete equation for arbitrary amplitude potentials, the difference between the two solutions was found to be not greater than 10% in regions of parameter space where the approximations used in obtaining the approximate solution were invalid.

Using the same model as Shukla et al. (1991), the existence of nonlinear potential structures in an homogeneous, magnetized dusty plasma was investigated in chapter 3. This was done by deriving a set of nonlinear equations describing the evolution of the system. Here the hot electrons have a Boltzmann distribution while the ions and the dust particles were represented by the fluid equations. In the linear limit, the system of equations produced a dispersion relation for coupled hybrid acoustic - drift waves.

Dipolar vortex potential structures and modified convective cell vortices in complementary regions of parameter space (Figure 3.1) were found to exist when the stationary solutions of the nonlinear equations were considered. These vortices might be responsible for enhanced particle and heat transport (in dusty plasmas in space, as well as in laboratory plasmas). An ensemble of such randomly distributed structures could constitute a new turbulent state. Furthermore a new range of low frequencies for fluctuation phenomena were found due to the presence of massive, charged dust grains.

In chapter 4, arbitrary amplitude dust-acoustic rarefactive and compressive solitons in an unmagnetized dusty plasma were studied. In this study the plasma model consisted of Boltzmann distributed electrons and ions (with two distinct groups of

thermal positive ions with different temperatures) and a negatively-charged, cold dust fluid whose dynamics were governed by the continuity and the momentum equations. It was found that in the absence of the electron component for both the rarefactive and the compressive solitons, the Mach number M should not become subsonic for soliton formation to be possible. In the rarefactive case, for $T_c/T_h = 0.05$, solitons were not found for $M > 1.159$, the upper limit in M being determined by the formation of double layer potential structures. Whereas for the compressive solitons, this value is determined by the condition that the dust density becomes complex. The dependence of the soliton amplitude (ϕ_m) on the cool to hot ion temperature ratio T_c/T_h for a given M value showed that for the compressive solitons the amplitude $\mid \phi_m \mid$ decreases with T_c/T_h and also there exists a lower threshold below which solitons do not occur. For the rarefactive solitons, the opposite behaviour was found.

Next, the effect of finite electron population was considered. When the electron density N_{eo} was varied for a given Mach number, it was found that the range of N_{eo} values in which the solitons occured was much larger in the case of the compressive solitons than for the rarefactive solitons. On the otherhand, the upper cut-off value of N_{eo} observed for the rarefactive solitons, was not seen in the compressive case. A variation of the soliton amplitude $\mid \phi_m \mid$ with the cool to hot ion density N_{co}/N_{ho} showed that the compressive solitons have a larger lower cut-off for soliton formation than the rarefactive solitons. Moreover the range of N_{co}/N_{ho} values over which the solitons were seen was found to decrease (increase) with the electron density for the former (latter).

The plasma model used in chapter 5 was that adopted in chapter 4. Here, study was made via the reductive perturbation technique of small amplitude solitons in a dusty plasma via both kinetic and fluid plasma models. A Vlasov-Possion system was used

for kinetic theory and the associated Korteweg de Vries (KdV) equation was derived. Then the fluid KdV equation was obtained by solving the basic set of fluid equations. When the kinetic and fluid KdV equations were compared, it was shown that the fluid equation could be obtained from the kinetic KdV equation if the coefficients α_k and γ_k were evaluated for a δ - function velocity distribution and thereby proved the consistent behaviour of the kinetic KdV equation. Since no thermal effects were considered in the fluid theory and no equilibrium drift was allowed in the kinetic approach, a comparison of the soliton profiles for both fluid and kinetic theory is not exact.

The work undertaken in this thesis lead to several avenues for extension. For example, the investigations of solitons in chapter 4 can be extended to thermal dust particles, as well as the inclusion of a confining external magnetic field. The studies in chapter 5 can be widened to include other forms of kinetic velocity distributions, especially those used to model beam - plasma interactions in space plasmas.

A limitation of our work is due to the treatment of the dust particles as being of constant charge. In reality, due to coagulation and fragmentation Z_d is changing. Thus the effects of non-constant dust charge will represent an important extension of our findings.

REFERENCES

[1] Angelis de, U., Formisano, V. and Giordano, M. 1988, J. Plasma Phys. **40**, 399.

[2] Baboolal, S., Bharuthram, R. and Hellberg, M.A. 1988, J. Plasma Phys. **40**, 163.

[3] Baboolal, S., Bharuthram, R. and Hellberg, M.A. 1990, J. Plasma Phys. **44**, 1.

[4] Bharuthram, R. and Shukla, P.K. 1986, Phys. Fluids **29**, 3214.

[5] Bharuthram, R. and Shukla, P.K. 1992a, Planet. Space Sci. **40**, 973.

[6] Bharuthram, R. and Shukla, P.K. 1992b, Planet. Space Sci. **40**, 465.

[7] Bharuthram, R. and Shukla, P.K. 1992c, Planet. Space Sci. **40**, 647.

[8] Bouchoule, A., Plain, A., Ph. Blondeau, L. and Laure, C. 1991, J. Appl. Phys. **70**, 1991.

[9] Carlile, R.N., Geha, S., O'Hanlon, J.F. and Stewart, J.C. 1991, Appl. Phys. Lett. **59**, 1167.

[10] Chen, F.F. 1974, *Introduction to Plasma Physics and Controlled Fusion* (2nd edition, vol. 1, Plenum, New York).

[11] D'Angelo, N. 1990, Planet. Space Sci. **38**, 1143.

[12] de Angelis, U., Formisano, V. and Giordano, M. 1988, J. Plasma Phys. **40**, 399.

[13] Garscadden, A. 1991, Invited lecture, XXth International Conference on Phenomena in Ionized Gases, Pisa, Italy, July 1991.

[14] Gendrin, R. 1991, Proc. XXth Int. Conf. on Phenomena in Ionized Gases: Invited Papers, pp. 14-25, Pisa, Italy.

[15] Goertz, C.K. 1989, Rev. Geophys. **27**, 271.

[16] Havnes, O. 1988, Astron. Astrophys. **193**, 309.

[17] Kato, y., Tajiri, M. and Taniuti, T. 1972, Phys. Fluids, **15**, 865.

[18] Kurth, W.S. 1991, Reviews of Geophysics Supp., p 1075, April 1991.

[19] Larichev, V.D. and Reznik, G.M. 1976, Dokl. Earth Sci. **231**, 12.

[20] Mace, R.L. and Hellberg, M.A. 1993, Planet. Space Sci. **41**, 235.

[21] Mak, S.S. 1992, Plasma Phys. and Cont. Fusion **34**, 453.

[22] Makino, M., Kamimura, T. and Taniuti, T. 1981, J. Phys. Soc. Japan, **50**, 980.

[23] Meiss, J. and Horton, W. 1983, Phys. Fluids **29**, 1828.

[24] Northrop, T.G. 1989, A Variety of Plasmas : Proc. 1989 Int. Conf. on Plasma Physics, p 91.

[25] Rao, N.N., Shukla, P.K. and Yu, M.Y. 1990, Planet. Space Sci. **38**, 543.

[26] Rosenberg, M. 1993, Planet. Space Sci. **41**, 229.

[27] Sagdeev, R. Z. 1966, Reviews of Plasma Physics (ed. M. A. Leontovich), Consultants Bureau, Vol. IV, p. 23.

[28] Sheehan, D.P., Carilo, M. and Heidbrink, W. 1990, Rev. Scient. Instrum. **61**, 3871.

[29] Shukla, P.K., Yu, M.Y. and Bharuthram, R. 1991, J. Geophys. Res. **96**, 21,343.

[30] Shukla, P.K. and Silin, V.P. 1992, Phys. Scripta **45**, 508.

[31] Taniuti, T. and Nishihara, K. 1983, Nonlinear Waves, p.100. Pitman.

[32] Verheest, F. 1993, Fourth Inter-national Symposium on double layers and other non-linear potential structures in plasmas, Innsbruck, Austria, July 6 - 8.

[33] Vidhya Lakshmi, S., Bharuthram, R. and Shukla, P.K. 1993, Astro. Space Sci. **209**, 213.

[34] Vidhya Lakshmi, S., Bharuthram, R. and Yu, M.Y. 1993, Astro. Space Sci. **209**, 71.

[35] Vidhya Lakshmi, S. and Bharuthram, R. 1994, Planet. Space Sci. **42**, 875.

[36] Whipple, E.C., Northrop, T.G. and Mendis, D.A. 1985, J. Geophys. Res. **90**, 7405.